REVIEWS IN ADVANCE

Lessons Learned from the 2004 Sumatra-Andaman Megathrust Rupture

Peter Shearer[1] and Roland Bürgmann[2]

[1]Institute of Geophysics and Planetary Physics, University of California, San Diego, La Jolla, California 92093; email: pshearer@ucsd.edu

[2]Department of Earth and Planetary Science, University of California, Berkeley, California 94720; email: burgmann@seismo.berkeley.edu

Annu. Rev. Earth Planet. Sci. 2010. 38:103–31

The *Annual Review of Earth and Planetary Sciences* is online at earth.annualreviews.org

This article's doi:
10.1146/annurev-earth-040809-152537

Copyright © 2010 by Annual Reviews.
All rights reserved

0084-6597/10/0530-0103$20.00

Key Words

subduction earthquakes, finite-slip inversion, tsunami warning

Abstract

The 2004 Sumatra-Andaman earthquake has been extensively studied because of its great size and devastating consequences. Large amounts of high-quality seismic, geodetic, and geologic data have led to a number of proposed models for its length, duration, fault geometry, rupture velocity, and slip history. The latest of these models vary in their details but now largely agree in their large-scale features, which include significant coseismic slip along the entire 1300- to 1500-km rupture, the bulk of which occurred fast enough to radiate seismic waves. The earthquake's enormous size has challenged conventional processing approaches and stimulated the development of new analysis and inversion methods, including multiple-source inversions, high-frequency body-wave imaging, and satellite observations of tsunami heights and gravity changes. The Sumatra megathrust earthquake was the largest in 40 years and is by far the best documented, but it does not seem fundamentally different in its properties from other large subduction-zone earthquakes.

INTRODUCTION

More than five years have passed since the devastating 2004 Sumatra-Andaman megathrust earthquake and tsunami. The size and importance of this earthquake, together with the many high-quality geophysical data sets that constrain its properties, have led to a large number of studies concerning various aspects of the event and its tectonic context. Many uncertainties regarding the nature of this earthquake that prevailed in the first few months have been resolved, such as the full size and extent of the rupture, which lasted 8 to 10 min and extended for 1300 to 1500 km, with a moment magnitude of 9.1 to 9.3. This makes it one of the largest earthquakes of the past century, smaller in moment only to the 1960 Chile and 1964 Alaska earthquakes, and the first great megathrust rupture to be recorded by modern broadband seismometers and global positioning system (GPS) equipment. However, issues remain concerning the exact geometry of the fault, including its depth and dip angle, and why such a large earthquake occurred along a section of plate boundary that was not widely thought to be at high risk for a M 9+ event.

Megathrust faults occur at locations where subducting oceanic lithosphere is thrust below continental margins and island arcs. The bulk of the world's seismicity occurs in these subduction zones, where, following the Gutenberg-Richter magnitude-frequency relationship, there are many more small earthquakes than large earthquakes, and few exceed moment magnitude (M_W) 8. On rare occasions, however, these events approach or exceed M_W 9. Because such great megathrust earthquakes involve slip over large fault widths (150 to 300 km) and lengths (500 to 1500 km), they are much larger than any earthquakes in the continental crust, and they release the bulk of the relative plate motion in subduction zones. Because they produce vertical seafloor motion over large areas, they often generate huge tsunamis, which greatly magnify their destructive potential. Prior to 2004, great megathrust earthquakes were thought most likely to occur in regions with relatively young oceanic crust subducting at high convergence rates (Ruff & Kanamori 1980); this occurred both for the 1960 $M_W \sim 9.5$ Chile and 1964 $M_W \sim 9.2$ Alaska earthquakes. However, the Sumatra-Andaman earthquake has forced a reevaluation of these theories (Kanamori 2006a, McCaffrey 2008, Satake & Atwater 2007), as it occurred in a region with older oceanic crust and relatively slow convergence rates, particularly within the northern part of its rupture zone.

The 2004 earthquake struck at the northern edge of the Sunda megathrust, where the Indian and Australian plates are subducting beneath the Sunda shelf (McCaffrey 2009) (see **Figure 1**). The relative plate motion near the epicenter is approximately 50 mm year^{-1} but is not perpendicular to the trench. The motion can be partitioned into two parts: a trench normal component associated with pure reverse faulting and a trench parallel component associated with strike-slip faulting. Additional complexity of the plate tectonic setting comes from the broadly distributed nature of the India-Australia plate boundary deformation zone between ~10°S and ~5°N latitude along the Sunda thrust (e.g., Delescluse & Chamot-Rooke 2006). The Sumatra subduction zone is considered a classic example of such slip partitioning, with much of the strike-slip motion occurring on the onshore Sumatran fault, continuing its northern extension into the West Andaman fault, and connecting with the Sagaing fault in Burma via several stepped mid-ocean-ridge segments (e.g., Curray 2005). The small Burma plate in the forearc between the subduction trench and the strike-slip fault is termed a sliver plate. Motion and deformation within the sliver plate control the relative amounts of reverse and strike-slip faulting along the subduction thrust fault and thus the slip vector directions of its earthquakes. As the Andaman-Nicobar section of the trench curves northward, it becomes nearly parallel to the relative plate motion (see **Figure 1**), reducing the convergence rate to less than approximately 20 mm year^{-1}, although this number is poorly known because of uncertainties in the amount of deformation within the Burma forearc sliver plate (e.g., McCaffrey 2009).

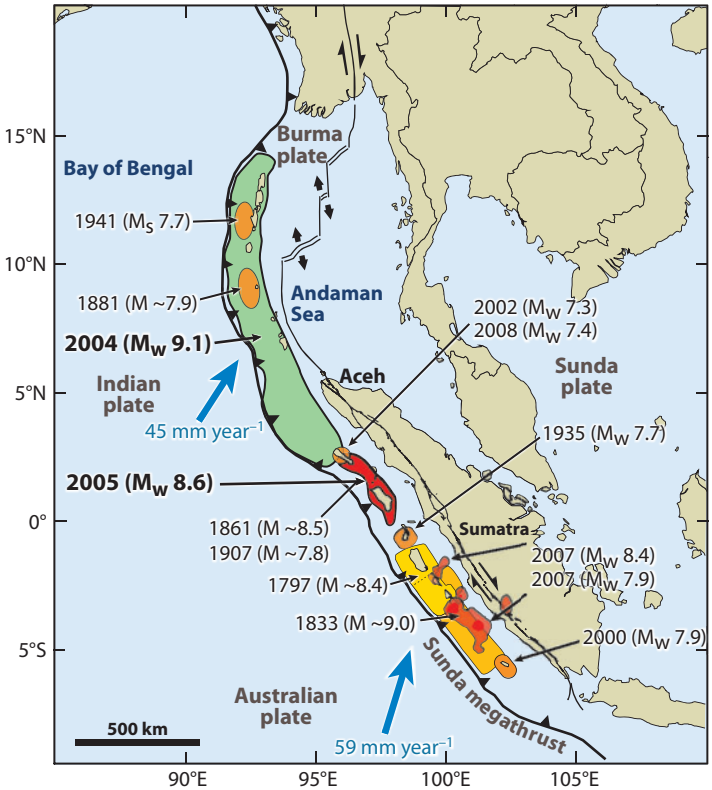

Figure 1

Tectonic context and earthquake history along the Sunda subduction zone. A forearc sliver (Burma microplate) separates the subducting Indian and Australian plates from the Sunda plate to the northeast. Labeled blue arrows indicate the rate and orientation of plate motions relative to the Sunda plate. Black lines delineate major plate-bounding fault zones in the region. Labeled colored outlines show the extent of large historic and recent ruptures on the megathrust. Data taken from Bilham 2005, Briggs et al. 2006, Konca et al. 2008, and Natawidjaja et al. 2006.

For all of the 2004 earthquake's scientific importance, it remains sobering to recall the tragic consequences of this event for the people of Sumatra and the Indian Ocean coastlines, where more than 200,000 were killed. Vertical motions on the seafloor generated a large tsunami, which caused most of the deaths by inundating coastal areas in northern Sumatra and around the Bay of Bengal. Except at Aceh and other sites on the northwestern tip of Sumatra, the tsunami waves traveled for 1 to 2 h before arriving at the impacted communities. Thus many deaths could have been prevented if an effective early warning system had been in place for the region. A technical challenge for providing prompt warnings regarding future great megathrust earthquakes and any tsunamis they generate is to develop algorithms that can recognize very large ($M_W > \sim 8.5$) subduction-zone earthquakes as rapidly as possible. The Sumatra-Andaman earthquake has spawned a number of new approaches to this problem, such as focusing on the first-arriving body-wave seismic phases, rather than relying on the slower traveling surface waves, and real-time analysis of distributed GPS stations operating at 1 Hz, which can directly measure coseismic signals.

A GIANT EARTHQUAKE

Seismic moment (M_0): a fundamental measure of earthquake size, defined as $M_0 = \mu A D$, where μ is the shear modulus of the rock in the source region, A is the fault area, and D is the average displacement (slip) on the fault

Moment magnitude (M_W): a logarithmic measure of moment, commonly defined as $M_W = 2/3\ (\log_{10} M_0 - 9.1)$, where M_0 is in newton meters

By any measure, the 2004 Sumatra-Andaman earthquake was one of the largest ever observed. Seismologists have many ways to characterize earthquakes, but the most important parameter for measuring earthquake size is the seismic moment, M_0, often expressed as the moment magnitude, M_W. Only rarely can the surface area and displacement of the fault be observed directly, so moment is typically estimated from records of radiated seismic waves or geodetic observations of permanent displacements caused by the fault movement. In both cases, instrumental advances over the past 20 years greatly improved our ability to study the Sumatra earthquake compared with previous great megathrust events. Seismic estimates of moment for large earthquakes require accurate measurements at very long periods (i.e., comparable to the rupture duration time), which are now provided by the broadband instruments of the global seismic networks, and geodetic moment estimates can now be made using GPS measurements, which are cheaper and more accurate than traditional surveying methods. Estimates of M_W for the Sumatra-Andaman earthquake range from approximately 9.1 to 9.3, with the limits corresponding to an uncertainty in moment of approximately a factor of two. This relatively large uncertainty arises from tradeoffs between the computed moment and the assumed fault dip and other near-source properties.

It is difficult to compare the properties of older great earthquakes in detail with the much more complete picture that we have of the Sumatra earthquake. However, their fault geometries can be roughly estimated from aftershock locations, which generally are observed to outline large-earthquake rupture zones. **Figure 2** compares the first month of aftershocks for the Sumatra earthquake with the 1957 $M_W \sim 9.0$ Aleutian, the 1960 $M_W \sim 9.5$ Chile, and the 1964 $M_W \sim 9.2$ Alaska earthquakes. The 2004 Sumatra-Andaman event has the longest aftershock zone—more than 1300 km—and an implied slip area that exceeds that of the Aleutian and Alaskan events and approaches that of the Chile event. The Chile earthquake appears to have had a larger fault width and a significantly larger moment.

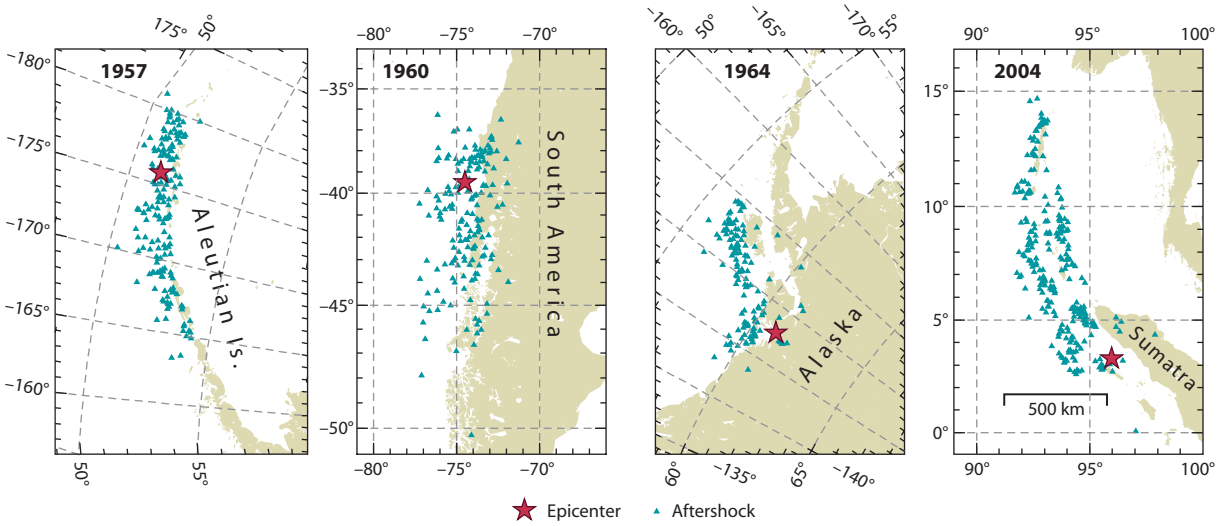

Figure 2

The first month of catalogued aftershocks for four great megathrust earthquakes. Red stars show the main-shock epicenters. All maps are plotted at the same scale. Figure modified from Ishii et al. (2005).

Table 1 Properties of great megathrust earthquakes

Earthquake	M_W	M_t	Length (km)	Duration	Vr (km s^{-1})
1957 Aleutian	8.5–9.0	9.0	~1200		
1960 Chile	~9.5	9.4	800–1000	250–340 s	~3.5
1964 Alaska	~9.2	9.1	500–700	250–340 s	~3.0
2004 Sumatra	9.1–9.3	9.1	1300–1500	500–600 s	2.0–2.8

Data taken from Abe 1979, Houston & Kanamori 1986, Ishii et al. 2005, and Kanamori 2006b.

Table 1 compares the basic properties of the four best-recorded great megathrust earthquakes of the past century. The Sumatra event stands out for its exceptionally long rupture length and duration and a relatively slow average rupture velocity. All these earthquakes generated major tsunamis, as indicated by their tsunami magnitude, M_t, a simple measure of tsunami size defined by Abe (1979). The size of the Sumatra tsunami is roughly that expected for an earthquake of its moment; its huge death toll resulted from the proximity and vulnerability of coastal populations rather than anything unusual about the tsunami itself.

DATA SOURCES

Study of the 2004 Sumatra-Andaman earthquake is greatly facilitated by advances in geophysical instrumentation since the last great megathrust event, the 1964 Alaska earthquake. These include upgrades to the seismic networks, as well as new technologies, such as GPS and satellite gravity.

Seismic and Hydroacoustic Data

The quantity, quality, and availability of seismic data have improved dramatically in the past 40 years. Older seismographs produced analog records, which would often clip on large earthquakes and had limited frequency response that prevented recording very long periods and normal modes. Modern stations in the global seismic networks produce digital, broadband, and high–dynamic range records, which are ideally suited to capturing the seismic radiation of M 9+ events. **Figure 3** shows the locations of the more than 400 global seismic stations that recorded the Sumatra earthquake. There are many more stations available from local and regional seismic networks.

Seismograms of the Sumatra earthquake vary greatly in appearance depending on their distance from the source, their displacement component, and the way in which they are filtered, as illustrated by the example traces in **Figure 3**. At 138° distance, the broadband vertical-component record from station CBN (Virginia, United States) is dominated by the PKP wave train (starting at ~20 min) and overtones (high-order surface-reflected body waves, starting at approximately 70 min). This high-frequency energy decays relatively rapidly with time, and little remains after several hours. However, if the record is filtered to 100 s and longer periods, then the SS and Rayleigh wave arrivals are most prominent. The Sumatra earthquake excited very long period energy (>1000-s period) that remained observable for many weeks as Earth's normal modes (free vibration periods) gradually decayed. The corresponding north-component record from the same station has more prominent SS and Love wave arrivals. At 70° distance, the broadband vertical-component record from station CASY (Antarctica) shows clear P, S, and Rayleigh wave arrivals. Filtering this record to frequencies above 0.5 Hz focuses on the P wave train because attenuation removes the shear and surface-wave arrivals. Because the earthquake ruptured northward and away from this station, a seismic directivity effect causes the apparent 12-min event duration in the seismogram to be somewhat longer than its true duration of 8–10 min. When a fault ruptures away from a seismic

PKP: a compressional wave that travels through Earth's core and arrives at distances beyond 100°

SS: a shear wave consisting of two surface-to-surface ray paths, connected by an underside reflection off the surface

P and S: direct compressional and shear arrivals, respectively, observed to source-receiver distances of up to 100°

Directivity: the sensitivity of seismic observations to the direction of fault rupture, in particular the dependence of the apparent event duration on the position of the recording station

station, the seismic waves from the ending point of the rupture have a longer distance to travel and an increased travel time compared with those that originate at the rupture starting point (the earthquake hypocenter). This increases the apparent duration of the event at the recording station. The opposite occurs when the earthquake ruptures toward a station—the apparent rupture

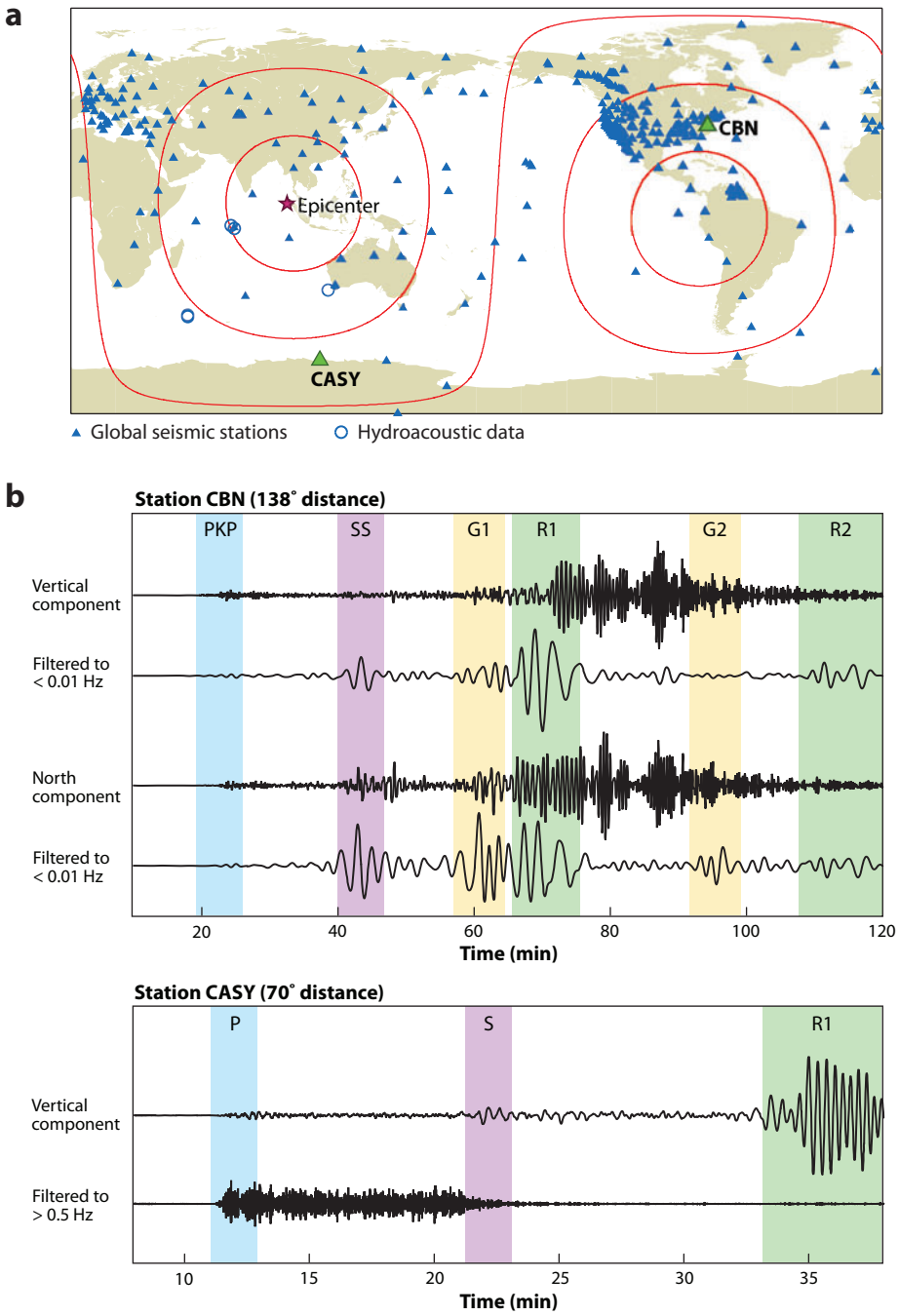

duration decreases. Analysis of seismic waves as a function of azimuth is one of the simplest ways to estimate the duration and rupture length of great earthquakes.

Geodetic Observations of Deformation and Gravity Changes

In recent decades, great advances have been made in efforts to observe and explain crustal deformation associated with earthquakes owing to improved space-geodetic measurements and deformation modeling programs. Advances in geodetic techniques, especially the increased precision and spatial and temporal coverage of GPS measurements (Segall & Davis 1997), have led to vast improvements in our ability to detect surface displacements associated with earthquakes. The existence of global networks of continuously operating GPS stations allows for the rapid characterization of large earthquakes from the measured surface motions. Complementing the GPS measurements of earthquake deformation for the 2004 Sumatra-Andaman earthquake are satellite measurements of gravity changes associated with the event, as well as field and remote sensing data of relative sea-level changes along the coastlines of the epicentral region.

The Sumatra-Andaman earthquake produced unusually large and far-reaching static surface displacements. Precise GPS measurements of coseismic monument motions come from continuously operating stations of regional and global (the International GNSS Service) networks, as well as from repeated survey-mode observations in GPS campaigns by various groups in the affected areas. Obtaining and combining the various data sets proved to be as challenging as the data and model analysis itself, given various limitations on data availability. A recent compilation of GPS offsets (Banerjee et al. 2007) incorporated measurements from 108 continuously operating stations (Banerjee et al. 2005, Hashimoto et al. 2006, Subarya et al. 2006, Vigny et al. 2005), measurements of 12 sites observed in survey mode before and after the event on the Andaman-Nicobar Islands (Banerjee et al. 2007, Gahalaut et al. 2006, Jade et al. 2005), 7 campaign-site offsets in Thailand (Vigny et al. 2005), and campaign measurements at 23 sites in northern Sumatra (Subarya et al. 2006). The vertical component of displacement is less well constrained than horizontal motions, and the composite data set of Banerjee et al. (2007) has 143 horizontal displacement vectors and 30 vertical offsets (**Figure 4**). Horizontal displacements from the earthquake exceeded 5 m at sites in northern Sumatra and the Nicobar Islands, located in the hanging wall of the coseismic rupture. Coseismic offsets were of order 1–2 cm in southern India, and still exceeded 5 mm at some stations located >3500 km from the rupture (**Figure 4**). The GPS data reveal a coherent surface motion roughly directed toward the earthquake rupture that can be detected out to distances of >5000 km from the epicenter (Banerjee et al. 2005, Kreemer et al. 2006).

Whereas continuous GPS measurements provide offset estimates for the day or even during the minutes of the earthquake (Blewitt et al. 2006, Vigny et al. 2005), survey-mode

←

Figure 3

Seismic stations recording the Sumatra earthquake and examples of waveforms. (*a*) The blue triangles on the map plot global seismic stations with records available through the IRIS data center. The blue circles show locations of hydroacoustic data. The red lines are at 30° intervals in distance from the main-shock epicenter. (*b*) Waveform examples from stations CBN and CASY are plotted below. Notice the changing character of these velocity records as a function of component and frequency. The body-wave phases P, PKP, S, and SS are labeled, as well as the surface waves G1 and G2 (Love waves, minor and major arc, respectively) and R1 and R2 (Rayleigh waves, minor and major arc, respectively). Because the source lasted more than 8 min, these seismic phases often appear as wave trains rather than distinct arrivals. For example, P begins at approximately 11 min in the lowermost trace, but P-wave energy from the rupture continues arriving past 20 min.

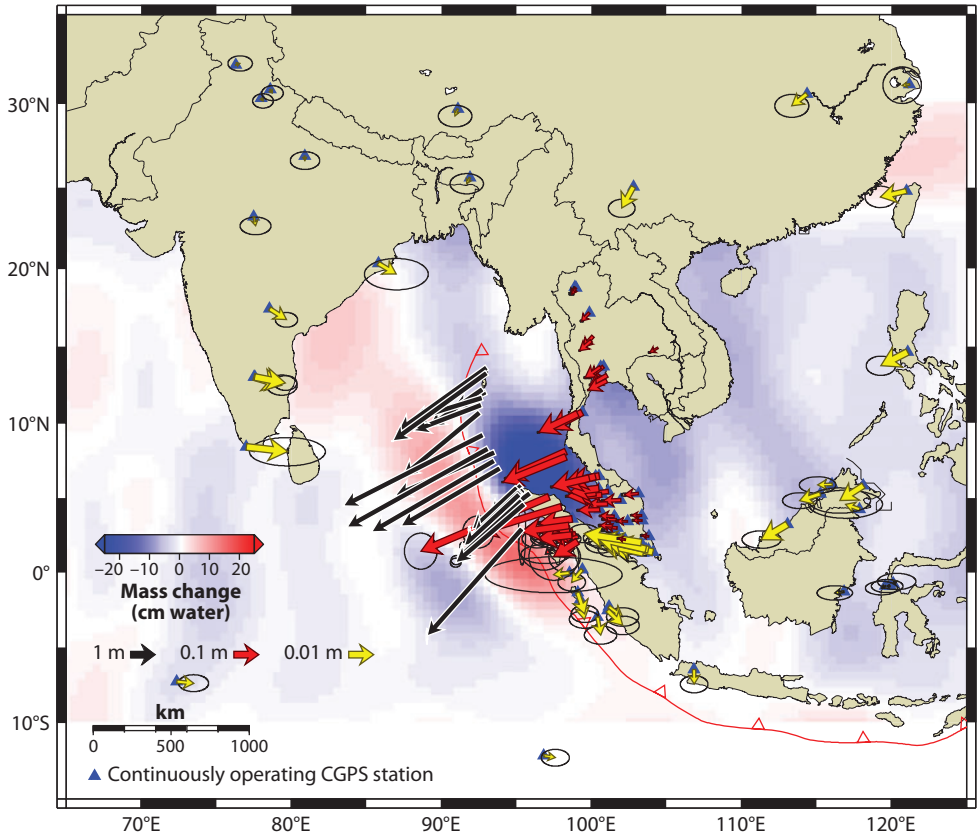

Figure 4

Coseismic GPS-measured static displacements and gravity changes from GRACE satellite measurements. GPS motions are displayed at three scales, different by a factor of 10, to allow for plotting of near-field, intermediate-distance, and far-field offsets. Arrows are tipped by 68% (1-sigma) confidence ellipses. (See Banerjee et al. 2007 for details on individual sources of data in this compilation.) Coseismic gravity changes (J. Wahr & S. Swenson, unpublished results) are color contoured. Values are mass change spanning the earthquake in centimeters of equivalent water thickness, calculated from GRACE time series data. Gravity data are not shown over landmasses for clarity.

observations may span days to years of pre-earthquake and postseismic deformation. Depending on the last/first time a survey-mode site was observed before/after the earthquake, corrections for interseismic/postseismic motions have to be made. Interseismic motions are relatively small compared with the early postseismic period, and they can be estimated either from pre-earthquake GPS measurements or using first-order locking models of the subduction thrust (Banerjee et al. 2007, Chlieh et al. 2007). Accounting for postseismic deformation that accumulates between the time of the coseismic rupture and the first subsequent observation requires continuous GPS data records or may involve subtracting predicted motions from time-dependent models of postseismic relaxation that are constrained by the sparse continuous station data and later measurements (Banerjee et al. 2007, Chlieh et al. 2007, Gahalaut et al. 2008b, Vigny et al. 2005) (see the section Postseismic Response, below).

Space-based measurements of temporal changes in Earth's gravity field from very large earthquakes are made possible with data from the GRACE (Gravity Recovery and Climate Experiment)

satellite mission launched in 2002. Precise measurements of the distance between and position of two identical satellites separated by ~220 km in 450-km-high orbits are used to determine Earth's gravity field at approximately monthly intervals and to improve our knowledge of time-variable mass distributions on Earth. The Sumatra-Andaman earthquake was the first earthquake to have its coseismic and postseismic gravity changes captured by the GRACE satellite (Chen et al. 2007, de Linage et al. 2009, Han et al. 2006, Ogawa & Heki 2007, Panet et al. 2007). The gravity-field disturbance from both the Sumatra-Andaman and subsequent March 2005 M_W 8.7 Nias earthquakes extends for nearly 1800 km along the Sunda-Andaman subduction zone. The gravity change includes a zone of gravity increase roughly west of the offshore trench and a zone of gravity decrease to the northeast in the Andaman Sea (**Figure 4**). The coseismic gravity change shown in **Figure 4** was computed using GRACE time series from April 2002 through February 2009 for which a trend, an annual cycle, a semi-annual cycle, and the offset at the time of the earthquake were estimated (J. Wahr & S. Swenson, personal communication). The map shows the amplitude of the offset, expressed as a change in surface mass, in units of centimeters of water thickness. Gravity changes away from the earthquake zone primarily represent unrelated redistributions of water mass.

Both the amplitude and wavelength of the coseismic gravity-change signal are strongly dependent on the degree and nature of filtering algorithms used in the analysis, and thus the estimates of the peak-to-peak gravity-change range widely from ~10 to 30 μGal (mass change equivalent of 24–72 cm of water). The relatively coarse spatial resolution of the gravity-change measurements (>400 km) provides a highly smoothed image of the coseismic changes, which must be taken into consideration when making comparisons with other data sets or models. The coseismic changes in the gravity field have contributions from vertical displacements of Earth's layered density structure and from density changes due to elastic volume strain in the lithosphere (Han et al. 2006), but they are also affected by associated ocean mass redistribution (de Linage et al. 2009). GRACE also detected significant postseismic gravity changes, consisting of a broad zone of gravity increase flanked by two smaller negative anomalies to the west and east (Chen et al. 2007, de Linage et al. 2009, Han et al. 2008, Ogawa & Heki 2007, Panet et al. 2007).

Additional information about static deformation from the earthquake comes from coastal vertical motions that can be determined by field studies of the response of corals to the change in local tide induced by coastal uplift/subsidence and by satellite imagery revealing changes in the coastal water depths (Kayanne et al. 2007, Meltzner et al. 2006). Meltzner et al. (2006) found that the zone of coseismic uplift extends from the middle of Simeulue Island at 2.5°N to Preparis Island at 14.9°N, suggesting an along-arc rupture length of as much as 1600 km. The pivot line dividing regions of uplift and subsidence is particularly useful to define the lateral extent and downdip limit of the rupture. Kayanne et al. (2007) use coral uplift data and changes in shoreline positions in the Andaman Islands to show that here the coseismic rupture terminated as much as 80 km east of the trench with its downdip limit 50 km further east, and that postseismic slip then propagated updip in subsequent months. The geologic uplift data proved valuable in inversions for coseismic slip models (Banerjee et al. 2007, Chlieh et al. 2007, Subarya et al. 2006).

Tsunami Observations

Within minutes after the earthquake, a powerful tsunami struck the coast near the northwestern tip of Sumatra. Wave heights reached 30–50 m along the western Aceh coast. The impact was most severe in Banda Aceh, the largest city in the region, where wave heights of 5 to 12 m were reported and more than 100,000 people were killed. Wave heights diminished at points further south along the southwest coast, but they were still large enough to be devastating to coastal communities

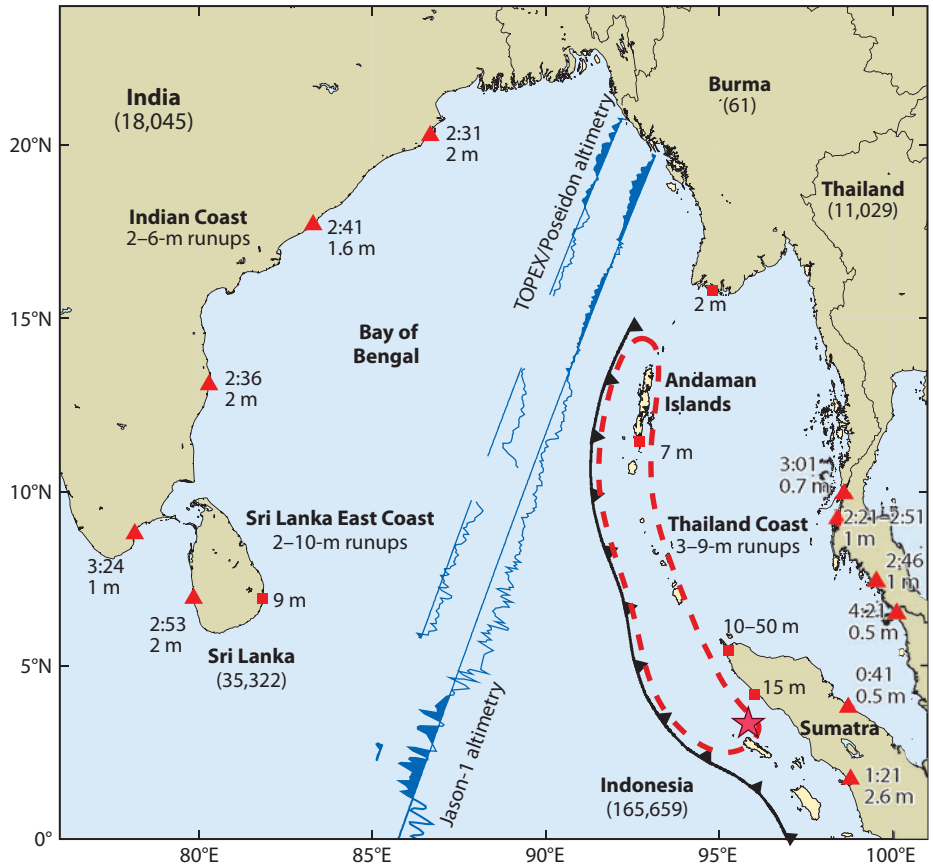

Figure 5

Summary of tsunami impact and data constraints. The Sumatra-Andaman earthquake epicenter and approximate rupture zone are shown by the red star and dashed line, respectively. The black line with wedges shows the trench location. The numbers of deaths are shown in parenthesis next to the country names. The red triangles are tide gauge records and are labeled with the tsunami arrival time (relative to the earthquake origin time) and peak amplitude. The red squares are selected tsunami runup amplitudes. The approximate range of runup values along various coastlines is also indicated. The blue lines show altimetry data from the Jason-1 and TOPEX/Poseidon satellites, at a time approximately 2 h after the earthquake. Positive amplitudes (higher sea surface) are shaded; the maximum plotted amplitude, near the south end of the Jason-1 profile, is 53 cm. This profile contains another, higher-amplitude, maximum of 66 cm, at a latitude of −4°, south of the map window. The death numbers and other data are derived from **http://www.ngdc.noaa.gov/hazard/tsu.shtml** and **http://nctr.pmel.noaa.gov/indo_1204.html** at the NOAA National Geophysical Data Center and the Center for Tsunami Research.

(e.g., 15-m runup at Meulaboh). Total deaths in Indonesia exceeded 165,000. Approximately 2 to 3 h later, the tsunami arrived at the coast of Thailand, India, and Sri Lanka (see **Figure 5**), generating runups of 2 to 10 m and tens of thousands of additional deaths. As the tsunami spread into the Indian Ocean, its amplitude slowly diminished, but runups of 2 to 3 m killed more than 100 in the Maldives islands, and runups of 6 to 9 m killed almost 300 in Somalia.

Runup observations depend strongly on near-coastal bathymetry and local site conditions and thus are not ideal for quantitative modeling of tsunamis. Most analyses of the 2004 tsunami have relied on tide gauge records, which provide a continuous measure of sea-surface height as

a function of time. Operating tide gauges near the Sumatra earthquake are plotted in **Figure 5**. Unfortunately, there were no gauges near Banda Aceh or in Burma, and a gauge at Port Blair in the Andaman Islands had timing problems (e.g., Neetu et al. 2005). These tide gauge records reported maximum amplitudes of 1 to 3 m, typically two to five times smaller than maximum tsunami runups from the same areas (Titov et al. 2005). The tsunami eventually spread throughout the world's oceans (e.g., Titov et al. 2005) and arrived on both coasts of the United States in 30 to 35 h with tide gauge amplitudes of 6 to 31 cm (**http://www.ngdc.noaa.gov/hazard/recenttsunamis.shtml**).

The tsunami is the first for which there are satellite altimetry profiles of wave height in the open ocean. The Jason-1 and TOPEX/Poseidon satellites crossed the region approximately 2 h after the earthquake and returned sea-surface elevation measurements that captured the leading edge of the tsunami wave as it exited the Bay of Bengal and entered the open Indian Ocean (see **Figure 5**). These data (corrected for tides, atmospheric pressure changes, and permanent oceanographic features such as eddies) provide first-order constraints on the tsunami waves.

KINEMATIC MODELS OF SLIP

Rapid slip on earthquake faults radiates seismic waves and results in permanent geodetic deformation of Earth's surface. Assuming models for Earth's elastic properties, geophysicists can compute Green's functions that provide the predicted seismic or geodetic response as a function of the slip on individual fault elements. They can use these to set up the inverse problem to estimate the spatial and temporal distribution of fault slip from seismic and geodetic observations (e.g., the timing and amplitude of various seismic phases and GPS static offset data). These slip models are purely kinematic because they make no assumptions regarding the causes of the motions, although they will often apply constraints to make the models more physically realistic (e.g., no backward slip). Seismic analyses can solve for the slip history, including parameters such as the rupture velocity, whereas GPS data generally constrain only the total slip from the entire earthquake. GPS data are ideally suited to detect slip at longer timescales than the seismically observed rupture duration, including the postseismic motions that last for many years after large earthquakes.

Table 2 lists the moment, M_0, and fault geometry for many studies of the Sumatra earthquake, and **Figure 6** shows the slip distribution for some of these models, which is discussed in the sections that follow. The maximum slip in the different models ranges from 11 to 35 m. The slip is linked to the earthquake moment by the local shear modulus at the fault; thus different amounts of model slip could result from different assumed values for the shear modulus, even if the moment remains constant. The models shown here use average shear modulus values that range from approximately 5 to 6.8×10^{10} Pa (often assumed to increase with depth), with the exception of Vigny et al. (2005), who use 4×10^{10} Pa. In addition to traditional seismic and geodetic analyses, the Sumatra earthquake slip is also constrained by satellite measurements of gravity changes (de Linage et al. 2009, Han et al. 2006, Panet et al. 2007), satellite and tide gauge measurements of the tsunami generated in the earthquake (Fujii & Satake 2007, Song et al. 2005), and observations of hydroacoustic waves (de Groot-Hedlin 2005, Guilbert et al. 2005, Tolstoy & Bohnenstiehl 2005).

Seismic Models

Inversion of seismograms for fault models is a long-standing activity in seismology. Small earthquakes are usually approximated as point sources because the available records are too far away to resolve any more details. In this case, only the total moment and geometrical properties such as the average fault orientation and slip direction can be resolved. These details are contained in centroid moment tensor (CMT) solutions for the source. However, for larger earthquakes,

Table 2 Moment estimates from seismic and geodetic studies

Study	Data	Fault dip	Moment (10^{22} N-m)	Max. slip (m)	Rupture velocity (km s^{-1})
Ammon et al. 2005 (model III)	20- to 500-s body and surface waves	12°/15°/17.5° (S to N)	6.5	11.4	~2
Stein & Okal 2005	Normal modes	8°	10		–
Tsai et al. 2005	Centroid moment tensor analysis	5.8–8.1°	11.7		4.1/3.0/3.3/2.2 (S to N)
Vigny et al. 2005	GPS	13°	7	34.2	3.7 to 2 (S to N)
Subarya et al. 2006	GPS + geologic	12°/15°/17.5° (S to N)	8.8		–
Pietrzak et al. 2007 (model 3)	GPS	Varies	5	33.9	
Chlieh et al. 2007	GPS + geologic	12°/15°/17.5° (S to N)	6.93	17.0	–
Banerjee et al. 2007	GPS + geologic	11–35°	7.62	19.4	–
Rhie et al. 2007	Seismic + GPS	11–18°	7.152	35.3	1.8 to 2.6
Vallee 2007	Rayleigh waves (empirical Green's function method)	16°	5.6		2.5 to 2.0 (S to N)

additional parameters related to the finite size of the fault can be obtained, such as the rupture length and duration and even the detailed time/space distribution of slip. These finite-slip models can be obtained from global earthquake records for events of $M \sim 7$ or greater.

There are few on-scale records close to the Sumatra earthquake, but because of its immense size, its rupture details can be readily resolved using data from the global networks (see **Figure 3**). The earthquake radiated seismic energy over a wide frequency band into a number of different seismic phases, including body waves (e.g., P and S waves) and surface waves (Love and Rayleigh), which arrive at different times in the seismogram because of their different propagation paths and velocities through Earth. Long-period (>20 s) body and surface waves are most useful for constraining seismic moment and slip details. High-frequency body-wave data can provide higher-resolution imaging of the rupture initiation point (the hypocenter), sources of seismic radiation along the rupture, and constraints on radiated energy, but they do not directly constrain the moment or the slip magnitude along the rupture. Thus the low-frequency seismic inversions are more directly comparable with the geodetic inversions, so we begin with them and defer discussion of the high-frequency results to later. For clarity, we do not discuss models that were later improved by the same group. For example, the multiple CMT analysis of Tsai et al. (2005) is more accurate than the initial Harvard single CMT solution.

Ammon et al. (2005) presented three different models based on inversions of long-period seismic data. Of these, model III is now most cited because it includes more of the northern part of the rupture and agrees better with subsequent studies. This model is derived from both body and surface waves; assumes three fault segments with dips of 12°, 15°, and 17.5° (south to north); and obtains a moment of approximately M_W 9.1. Several subsequent models have assumed the same basic fault geometry. One of the first papers to show the true size of the Sumatra earthquake was the normal-mode analysis of Stein & Okal (2005), who found that M_W 9.3 was required to explain the lowest-frequency normal modes. Tsai et al. (2005) showed that the large size and duration of the Sumatra earthquake could not be properly modeled with a single CMT, but that the seismic data are well explained by a series of five CMT solutions that mimic a northward

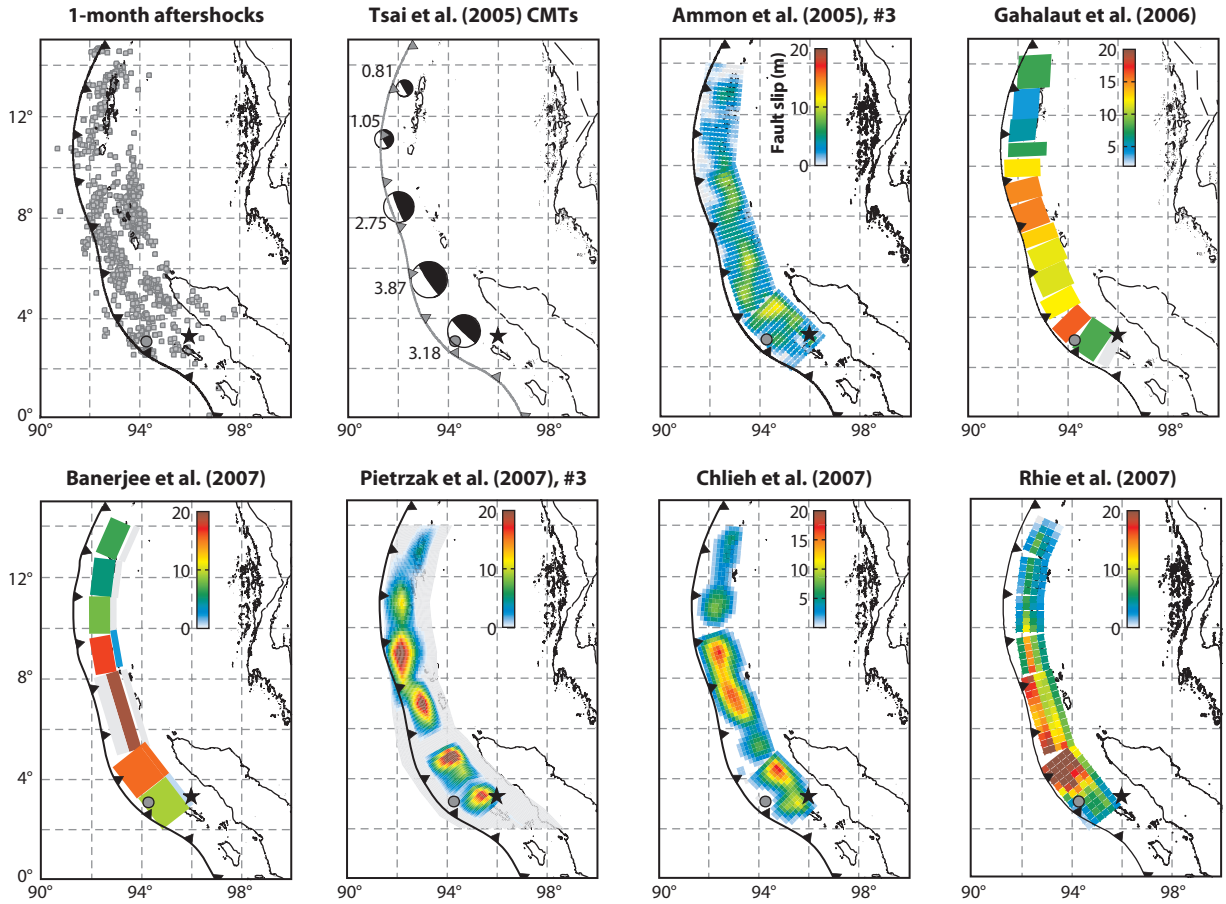

Figure 6

Published finite-slip models of the 2004 Sumatra-Andaman earthquake compared with the distribution of the first month of aftershocks (Engdahl et al. 2007) and the multiple centroid moment tensor (CMT) solution of Tsai et al. (2005) (see **Table 2** for details about the models). The black star shows the location of the earthquake hypocenter, and the gray circle shows the original single CMT location. These plots and the compilation of slip models are courtesy of Martin Mai (**http://www.seismo.ethz.ch/srcmod/**).

propagating slip pulse and have a total moment of M_W 9.3. Stein & Okal (2007) later showed that this model also fits the normal modes quite accurately, with its time dependence explaining an apparent increase in moment with normal-mode period that had led Stein & Okal (2005) to speculate about possible slow slip in the northern part of the rupture (see discussion below). Lambotte et al. (2006, 2007) used normal-mode phase measurements to estimate the rupture length and duration, obtaining ~1250 km and ~550 s. Braitenberg & Zadro (2007) found that normal modes recorded by a long-base tiltmeter in Italy at 0.3 to 3 mHz were 1.5 to 3 times greater for the 1960 Chile earthquake than for Sumatra event. Vallee (2007) used an empirical Green's function approach to model the Rayleigh waves from the Sumatra earthquake as a sum of waves from a M_W 7.2 foreshock in the same region and obtained an M_W of approximately 9.1.

Seismically derived moment estimates for the Sumatra earthquake range from 5.6 to 11.7 $\times$ 10^{22} N-m (see **Table 2**), corresponding to $M_W = 9.1$ to 9.3. Much of this factor-of-two uncertainty comes from differences in the assumed fault dip. Very shallow fault dips produce less seismic

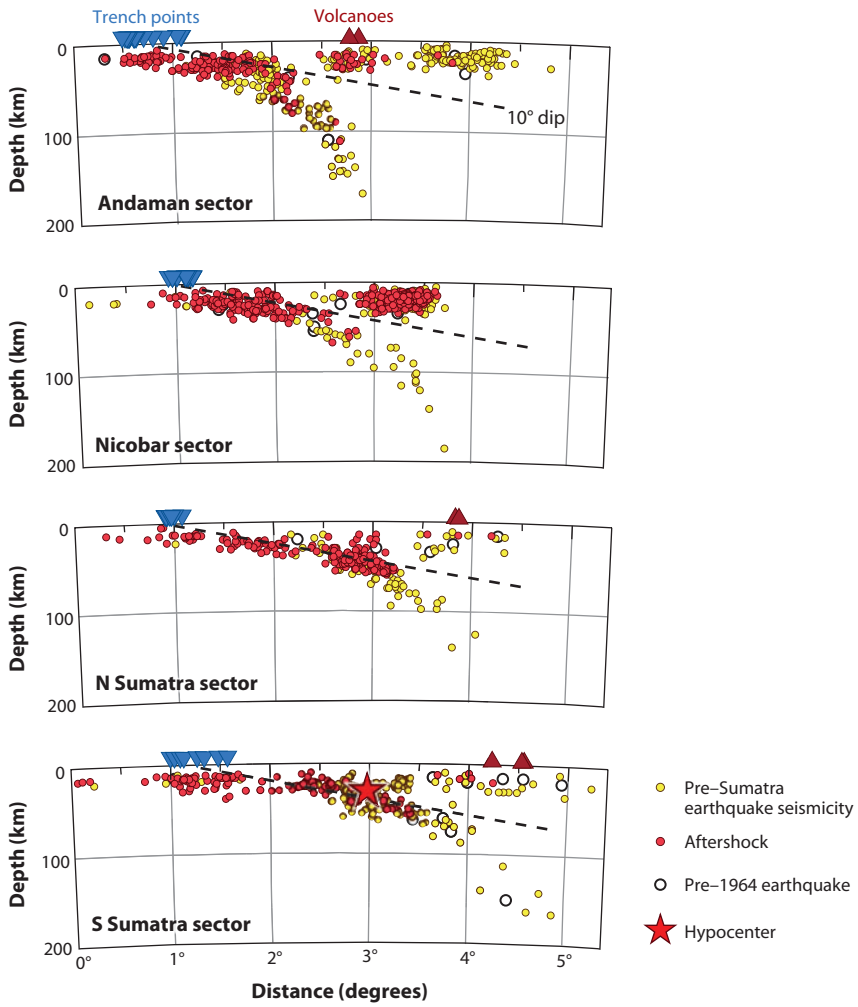

Figure 7

Cross sections of earthquake locations from Engdahl et al. (2007). Pre-Sumatra earthquake seismicity is shown in yellow, and aftershocks are plotted in red. The red star shows the hypocenter location. For reference, the dashed line shows a hypothetical 10° dipping slap interface intersecting the surface at the approximate trench location on the seafloor.

radiation for the same moment, and thus models with shallow fault dips (e.g., Tsai et al. 2005) tend to have higher moments than those with steeper dips (e.g., Ammon et al. 2005). Because it is difficult to resolve the fault dip directly in these inversions, the fault geometry is often specified based on other constraints, such as background seismicity and aftershock locations (e.g., Dewey et al. 2007, Hayes & Wald 2009). Unfortunately, despite efforts to improve these locations (e.g., Araki et al. 2006, Engdahl et al. 2007), their depth uncertainties remain too large to definitively constrain the geometry of the subduction interface (see **Figure 7**). It does appear likely, however, that the slab dip increases for the northward part of the rupture zone, as is included in most of the models.

A related issue is whether secondary coseismic thrust faulting may have occurred near the trench and if the subduction interface is currently below the oceanic crust, as some reflection seismic data suggest (Singh et al. 2008). There is also some evidence that there may have been a secondary source involving rupture of a splay thrust in the Aceh basin to account for the large tsunami runups observed in Aceh province (Banerjee et al. 2007, Plafker et al. 2006, Sibuet et al. 2007).

Inversions of Geodetically Measured Surface Displacements and Gravity Changes

The elastic deformation of Earth from fault slip in an earthquake produces static surface displacements and changes in gravity. Geodetic measurements of these motions and gravity changes can be used to calculate the size of the event and derive kinematic rupture models, independent of the seismic energy released by the earthquake. Obtaining quantitative information about the fault geometry and the distribution of slip of an earthquake rupture from surface deformation or gravity changes requires mechanical modeling.

Computer models are used to calculate the deformation of an idealized representation of Earth. Crustal deformation modeling benefits from ever-improving computational hardware and the development of advanced analytical and numerical model programs that allow for consideration of increasingly complex and realistic model geometry, boundary conditions, and material properties and for formal inversion of optimal rupture model parameters. In particular, for an event of the size of the Sumatra-Andaman earthquake, it becomes important to take into account the change in elastic properties with depth, as well as the spherical shape of Earth. Banerjee et al. (2005) showed that, because of an increase in rigidity with depth, predicted displacements from thrust faulting on a realistically layered sphere fall off with distance much more rapidly than those calculated on a homogeneous sphere. For stations at a >1000-km distance from the rupture, model displacements on a sphere are several times larger than those for homogeneous flat-Earth models. There is also a strong tradeoff between fault dip and scalar moment of a geodetic megathrust slip model; that is, estimates of seismic moment derived from fitting a given set of displacements are larger when more shallowly dipping planes are specified (Banerjee et al. 2005). Masterlark & Hughes (2008) argued that it is also important to account for the substantial three-dimensional heterogeneity of material properties across the subduction zone, which requires utilization of numerical finite-element-model techniques. Whereas some studies only compare forward predictions of existing slip models with observations, formal inversion methods are commonly used to find the optimal set of model parameters (i.e., the slip distribution) that best fit the observables. Similar to seismic inversions, additional constraints such as limits on the range of model-slip orientations, bounds on the total moment or maximum slip amplitudes, and the roughness of the obtained slip distribution are sometimes imposed during the inversion.

The far-field (>∼400-km distance from the rupture) continuous GPS station offset data can be fit well with simple models involving uniform slip on two to five dislocation planes (Banerjee 2005, Hashimoto et al. 2006, Kreemer et al. 2006, Vigny et al. 2005). The near-field survey-mode GPS and geologic observations allow for more refined slip models (**Figure 6**) (Banerjee et al. 2007, Chlieh et al. 2007, Gahalaut et al. 2006, Pietrzak et al. 2007, Subarya et al. 2006). Vigny et al. (2005) introduced a displacement field involving data from far-field continuous GPS sites and relied on uniform elastic half-space calculations to find that the peak slip zone on the rupture is located approximately 200 km northwest of the epicenter, with a second area of high slip near 9–12°N. Their analysis of 30-s GPS time series showed that stations in northern Thailand reached their final positions less than 10 min after the earthquake, providing an argument against the hypothesis of a largely aseismic northern rupture continuation. Gahalaut et al. (2006) used the

horizontal and vertical coseismic offsets of 13 survey-mode sites on the Andaman and Nicobar Islands to estimate (by trial and error) coseismic slip on 14 adjacent fault segments in an elastic half-space. Subarya et al. (2006) examined both layered and homogeneous half-space models to invert data from mostly near-field GPS stations, as well as field and remote sensing estimates of vertical motions. They found slip exceeding 20 m offshore northern Sumatra, with additional high-slip patches exceeding 10 m up to 14° N and a rupture extent of at least 1400 km. Pietrzak et al. (2007) used elastic half-space models and inverted for several slip models using different fault geometries and GPS and geologic uplift data subsets. The model shown in **Figure 6** is based on inversion of the data of Vigny et al. (2005) plus near-field data from other studies (Bilham et al. 2005, Gahalaut et al. 2006, Subarya et al. 2006) without correction for postseismic deformation.

Chlieh et al. (2007) used a model with a vertically layered elastic Earth structure to invert data from survey-mode and continuous GPS sites out to 1100 km from the rupture and near-field geologic data. They compared inversions of only continuous GPS data (located >400 km from the rupture) with models derived from near-field survey-mode measurements that span 20 to 40 days of postseismic motion to argue that afterslip of ∼30% of the coseismic moment added to the near-field displacements. From a joint inversion of the far-field and uncorrected near-field data, Chlieh et al. (2007) obtained a relatively detailed slip distribution with multiple peak-slip patches (**Figure 6**). Banerjee et al. (2007) analyzed both near- and far-field GPS data, taking into account both vertical rigidity layering and Earth sphericity, and corrected near-field GPS offsets for postseismic motions by subtracting predicted motions from a model of afterslip derived from the continuous data. They found that only ∼8% of survey-mode station offsets occurred in the first 20–40 days of postseismic deformation and that adding model slip on steeper dipping segments at depth can improve the fit to the near-field GPS deformation data, especially in the vertical component. The coarser, unsmoothed slip model of Banerjee et al. (2007) (**Figure 6**) has the same first-order features as models by Chlieh et al. (2007) and Ammon et al. (2005), including deep dip slip of ∼20 m near 4°N, relatively deep dip slip on the Nicobar segment from 5°N to 8°N, and 3–8 m of oblique slip along the Andaman Islands north of ∼9°N.

Gravity-change measurements by the GRACE satellite reveal a notable signal associated with the earthquake. Given the confounding factors of low spatial resolution and difficulties with removing contributions by nontectonic processes, the gravity data do not resolve any additional details of the rupture kinematics in models of the coseismic rupture. However, model analyses of the data show contributions to coseismic gravity changes from not only vertical displacements of the layered Earth (primarily the surface but also of the Moho and other interfaces between layers of different densities), but also elastic density changes (Han et al. 2006) and lateral shifts of ocean water mass (de Linage et al. 2009). To first order, the observed coseismic gravity changes are consistent with models derived from seismic and/or geodetic model inversions (de Linage et al. 2009, Han et al. 2006, Panet et al. 2007).

Tsunami Generation and Megathrust Slip

Great megathrust earthquakes produce vertical motions of the seafloor that can generate large tsunamis, which then propagate through the ocean in a complicated way that depends on details of the coastlines and the water depth. In principle, the bathymetry is known well enough that numerical modeling methods can accurately account for propagation effects, in which case the tsunami observations (e.g., tide gauge and satellite records) can be related directly to the model (the vertical motions of the seafloor, or often the slip model that causes these motions). For the Sumatra earthquake, this modeling has taken two different forms: (*a*) testing seismic or geodetic models of the earthquake to see how well they predict the tsunami observations (Geist et al. 2007,

Pietrzak et al. 2007, Titov et al. 2005) or (*b*) attempting to invert the tsunami observations for a fault slip model (Fujii & Satake 2007, Piatanesi & Lorito 2007, Song et al. 2005). Because of the large size of the Sumatra earthquake, point source models are not adequate, and the full length and duration of the event must be taken into account.

Some early tsunami modeling efforts were flawed by unrecognized timing errors at the Port Blair tide gauge. Neetu et al. (2005) pointed out this problem, using the timing of the tsunami arrival at Indian tide gauge stations to argue that the tsunami source region must extend at least to the Andaman Islands, 900 km north of the epicenter. Titov et al. (2005) and Geist et al. (2007) performed numerical simulations to show that models based on seismic and geodetic data that included slip extending to the Andaman Islands could fit most of the tsunami observations. Geist et al. (2007) showed that the tsunami observations were generally better explained by a 1600-km-long fault than a 900-km-long fault, assuming M_W 9.14 in both cases, although the model underpredicts the extreme runups at Banda Aceh. Fujii & Satake (2007) inverted tide gauge and satellite altimetry data for a slip model. Their preferred model has a 900-km-long fault and an average rupture velocity of 1 km s^{-1}, although a 1400-km-long source better fits the satellite data alone. They argued that substantial slip near the Andaman Islands would overpredict amplitudes at Indian tide gauge stations. Piatanesi & Lorito (2007) found that Sumatra tsunami amplitudes are not accurately approximated as a linear function of slip amplitude and applied a nonlinear inversion method based on a hybrid L1/L2 norm (for robustness with respect to data outliers) to tide gauge observations. Their best fitting model has three high-slip segments, one at the south end of the rupture, one at approximately 8°N, and one at approximately 12°N, and an average rupture velocity of 2.0 km s^{-1}. This model does, however, overpredict tide gauge amplitudes at the Indian tide gauge station Chennai, one of the two stations cited by Fujii & Satake (2007) as arguing against slip in the northernmost part of the rupture.

The existing tsunami modeling studies are not in complete agreement regarding the length of the best-fitting source region and the rupture velocity. However, given the limited data, we should not expect slip inversions based on tsunami data alone to have resolution comparable with the seismic and geodetic inversions.

Integrated Analyses and Joint Inversions

The Sumatra earthquake is constrained by an unprecedented variety of geophysical data. However, it can be difficult to compare results of individual studies because of differences in their modeling assumptions (e.g., fault location and geometry, local shear modulus). Several studies have taken a more integrated approach, either by testing models derived from one type of data by calculating predicted results for other data types or by performing joint inversions of multiple data types.

Song et al. (2005) considered models from seismic waveforms and satellite altimetry data to argue that models based on the two data sets produce consistent descriptions of the source of the event and resultant tsunami. Pietrzak et al. (2007) compared a suite of slip models derived from GPS offsets and geologic uplift data (Subarya et al. 2006) with tide gauge arrival times and the Jason-1 altimetry data of tsunami heights in the Indian Ocean (**Figure 5**). The temporal evolution of the slip was constrained by the 30-s GPS time series of Vigny et al. (2005). Pietrzak et al. (2007) argued that the tsunami data favor models with slip maxima that are as high (~20 m) in the northern portion (near 8–10°N) of the rupture as in the south (3–5°N) and that constructive interference of waves from the southern and northern high-slip patches further strengthened the tsunami along the Indian and Sri Lankan coasts.

Chlieh et al. (2007) focused on inversions of GPS data but considered a number of other geophysical constraints. They showed that their preferred coseismic slip model, which is grossly similar

to Ammon et al.'s (2005) model III, has three bursts of energy that agree with high-frequency analyses, predicts best-fitting double-couple moment tensors that agree with the multiple CMT analysis of Tsai et al. (2005), correctly predicts observed normal-mode amplitudes (if a rupture velocity of 2.2 to 2.6 km s^{-1} is assumed), roughly matches observed long-period surface-wave amplitudes, and does a reasonable job of predicting the tsunami amplitudes seen in the satellite altimeter data. For the seismic comparisons, they found that fixed rupture velocities of 2 to 2.6 km s^{-1} provide the best fits. They concluded that there is no need for aseismic slip in the Andaman Island region to reconcile the geodetic and tsunami results with seismic-wave modeling.

Rhie et al. (2007) considered a number of different models based on single and joint inversions of long-period seismograms and GPS data. They obtained approximately 30% more moment for the purely geodetic inversions than the purely seismic inversions, but they obtained a reasonable fit to both data types using a joint inversion approach and speculated that at least some of the mismatch in the individual inversions may result from incomplete removal of postseismic signal from the near-field GPS data. They noted that their results are sensitive to the assumed fault geometry and that the higher moment in Tsai et al.'s (2005) multiple CMT analysis results from a shallow fault dip angle. Rhie et al. (2007) showed that the fault dip angle is not well resolved in their inversions, but they prefer a steeper dip angle to be more compatible with the aftershock data. They found that average rupture velocities between 1.8 and 2.6 km s^{-1} can fit the seismic data.

SLOW SLIP ON NORTHERN SEGMENT?

Seismic and geodetic estimates of moment should agree, provided the slip is fast enough to be fully captured by seismic records and the geodetic estimates have the time resolution to capture only the coseismic slip and not any of the postseismic deformation that follows large ruptures. In the initial months following the Sumatra-Andaman earthquake, there was speculation that much of the moment released in the northern part of the rupture occurred at an intermediate timescale—as slow slip that did not radiate observable seismic waves but was still rapid enough to appear as coseismic moment release in geodetic observations (Bilham 2005, Lay et al. 2005). This was suggested by the initial Harvard CMT and some of the early finite-slip models from seismology that did not have substantial moment release to the north, as well as a tide gauge record at Port Blair and some tsunami modeling that suggested delayed vertical movements near the Andaman Islands. The existence of slow slip, if it could be confirmed, would be an important result with profound implications for other megathrust earthquakes. There is some evidence that the 1960 Chile earthquake was preceded by a slow-slip event of comparable moment (Cifuentes & Silver 1989), and slow earthquakes are now recognized as a common occurrence just below the locked part of subduction zones (Ito et al. 2007, Rogers & Dragert 2003).

However, initial seismic analyses of the Sumatra earthquake were based on algorithms that were not designed for an event of 500-s duration. The multiple CMT analysis of Tsai et al. (2005) and a number of other inversions later indicated substantial coseismic moment release along the northern segment. In addition, the Port Blair tide gauge record was found to have a timing error that accounted for its apparent delayed response to the earthquake (Neetu et al. 2005). Current coseismic slip models can largely explain both the geodetic and seismic observations (e.g., Chlieh et al. 2007, Rhie et al. 2007), as well as tsunami observations (Chlieh et al. 2007). However, there is a moment excess in some of the geodetic inversions compared with seismic inversions. It can be problematic to perform such comparisons between different studies because they often assume different fault geometries, which will yield different moment estimates even from the same set of observations. For their preferred fault geometry, Rhie et al. (2007) found that a GPS-only

inversion produced a 35% higher moment than a seismic-only inversion. On its face, this might argue for a component of slow slip at timescales longer than 500 s (the longest surface-wave periods used in the inversion), but this interpretation is not supported by evidence described in the next paragraph.

Vigny et al. (2005) examined continuous GPS records for the first few hours following the earthquake and found no signal for slow slip following the coseismic offsets. High-frequency and hydroacoustic studies show continuous rupture and high-frequency radiation extending to the northern end of the rupture. In addition, both Rhie et al. (2007) and Chlieh et al. (2007) have obtained models that fit both the geodetic and seismic data reasonably well, so the data do not appear to strongly require a moment difference. To place the Sumatra results in perspective, it is not unusual for separate seismic and geodetic inversions to yield different moment estimates. Often the geodetic inversions yield higher moments; this has been observed for the 1984 Northridge, the 1999 Chi-Chi, and the 2004 Parkfield earthquakes (Langbein et al. 2006). A possible explanation for these discrepancies is that the geodetically estimated moments may include significant postseismic deformation occurring immediately after the main shocks (although the Sumatra studies have attempted to correct for this effect). Of course, at some point this becomes a matter of semantics—we could term some of the rapid postseismic deformation immediately following a main shock to be a slow-slip event. But there is no evidence from the Sumatra earthquake that there was a distinct slow-slip event or that the rupture and postseismic response involved any exotic behavior different from that commonly observed for other earthquakes.

HIGH-FREQUENCY SEISMIC AND HYDROACOUSTIC OBSERVATIONS

Seismic observations that contribute to moment estimates and finite-slip models are made at relatively long periods (>20 s). Some of the finite-slip models discussed above included rupture velocity estimates, which range from approximately 2 to 3 km s^{-1} averaged for the entire event, with some evidence for slightly slower rupture velocities for the northern part of the rupture compared with the southern part. It is important to recognize that these long-period seismic estimates are often derived from time/space points that correspond to slip velocity maxima, and they may not reflect the actual onset of slip at a given point on the fault.

In addition to traditional finite-slip modeling, the Sumatra rupture has been studied by new techniques that exploit high-frequency (i.e., >0.2 Hz) P-wave and hydroacoustic arrivals (see **Table 3**). Ni et al. (2005) examined P-wave envelopes and applied a simple directivity model to show that the Sumatra rupture was approximately 1200 km long and lasted ~500 s, corresponding to an average rupture velocity of 2.5 km s^{-1}. Ishii et al. (2005) applied back-projection to P waves recorded by the 500-station Japanese Hi-Net array to image high-frequency radiation from the

Table 3 Rupture estimates from high-frequency seismic and hydroacoustic studies

Study	Data	Length (km)	Duration (s)	Velocity (km s^{-1})
Ni et al. 2005	P-wave envelopes	1200	500	2.5
Ishii et al. 2005	P-wave back-projection	1300	480	2.8
Kruger & Ohrnberger 2005b	P-wave beam forming	1150	480–500	2.3–2.7
Lomax 2005	P-wave ending times	1100	480	2.3
de Groot-Hedlin 2005	Hydroacoustic	–	–	2.4/1.5 (S to N)
Guilbert et al. 2005	Hydroacoustic, seismic array	1235	515	2.7/2.5/2.0 (S to N)
Tolstoy & Bohnenstiehl 2005	Hydroacoustic	1200	480	2.8/2.1 (S to N)
Gusev et al. 2007	P-wave envelopes	1020–1465	540–560	2.25

rupture as it propagated northward for 1300 km at an average rupture velocity of approximately 2.8 km s^{-1}. Kruger & Ohrnberger (2005b) used beam forming on P waves recorded by German stations to resolve a 1150-km-long rupture and an average rupture velocity of 2.3 to 2.7 km s^{-1}. Lomax (2005) estimated the ending times of the P wave train and applied a location algorithm to find the best-fitting rupture termination point and time, obtaining a 1100 $\pm$ 300-km-long fault and a duration of approximately 8 min. Gusev et al. (2007) analyzed high-frequency P-wave power recorded by global seismic stations and used an aftershock as an empirical Green's function to account for the expected shape of P-coda envelopes. They obtained a rupture length of 1241 $\pm$ 224 km and an average rupture velocity of 2.25 km s^{-1}. Many of these seismic studies indicate two to three distinct bursts of high-frequency radiation from the Sumatra earthquake (Ammon et al. 2005, Ishii et al. 2005, Kruger & Ohrnberger 2005a), at approximately 80, 320, and 480 s after the origin time, which roughly correspond to peaks in the moment release observed in long-period studies (Ammon et al. 2005, Tsai et al. 2005).

P waves couple into acoustic waves in the ocean, which can become trapped in the marine low-velocity channel and propagate for long horizontal distances as tertiary (T) phases. Hydrophone arrays in the Indian Ocean recorded T phases from the Sumatra earthquake, which were analyzed by de Groot-Hedlin (2005), Guilbert et al. (2005), and Tolstoy & Bohnenstiehl (2005). These studies indicated a rupture length exceeding 1200 km and rupture velocities of 2 to 2.7 km s^{-1}, with lower values for the northern part of the fault. [Tolstoy & Bohnenstiehl (2006) argued that the somewhat slower velocities obtained by de Groot-Hedlin 2005 are likely an artifact caused in part by neglecting azimuthal differences in the P-wave path compared with the T-phase path.] Seismic and acoustic studies that have attempted to solve for a variable rupture velocity generally obtain somewhat lower velocities for the northern part of the rupture, although in most cases the northern rupture velocity is still at least 2 km s^{-1}. However, Bilek (2007) found no evidence that smaller earthquakes in the northern fault portion have anomalously long durations, so this difference does not appear to reflect general variations in fault-zone character.

A fundamental constraint on rupture dynamics is provided by the total radiated seismic energy, E_R. Unfortunately, accurately estimating the radiated energy for earthquakes is difficult because P and S waves must be well-sampled over all takeoff angles and frequencies, and corrections for attenuation are critical. Studies of the same earthquake often yield differing energy estimates, and the Sumatra earthquake is typical in this respect. Lay et al. (2005) obtained $E_R = 1.1 \times 10^{17}$ J from teleseismic P waves. Kruger & Ohrnberger (2005a) obtained E_R estimates of 5.5 and 15.3×10^{17} J from German and Japanese network data, respectively. Kanamori (2006c) obtained $E_R = 3.0 \times 10^{17}$ J using Ammon et al.'s (2005) model III for low frequencies and observations of the P wave train at higher frequencies (extended to S waves using an assumed S/P energy scaling relationship). Choy & Boatwright (2007) analyzed the teleseismic P wave train, using reference events to correct for the amount of extra energy arriving in their 10-min window from other seismic phases, and obtained $E_R = 1.4 \times 10^{17}$ J. Both of these studies found that the second half of the rupture radiated less seismic energy than the first half. Using $E_R = 3.0 \times 10^{17}$ J and $M_0 = 6.5 \times 10^{22}$ N-m (Ammon et al.'s 2005 model III value), the energy moment ratio is 4.6×10^{-6}, a value comparable with that of other subduction-zone earthquakes, although slightly on the low side (Kanamori 2006c).

Postseismic Response

Continued GPS measurements following the Sumatra-Andaman earthquake showed strongly perturbed motions, both in the near-field and at greater distances in Indonesia and Thailand (**Figure 8**). GPS sites on the Andaman-Nicobar islands generally continued to move to the

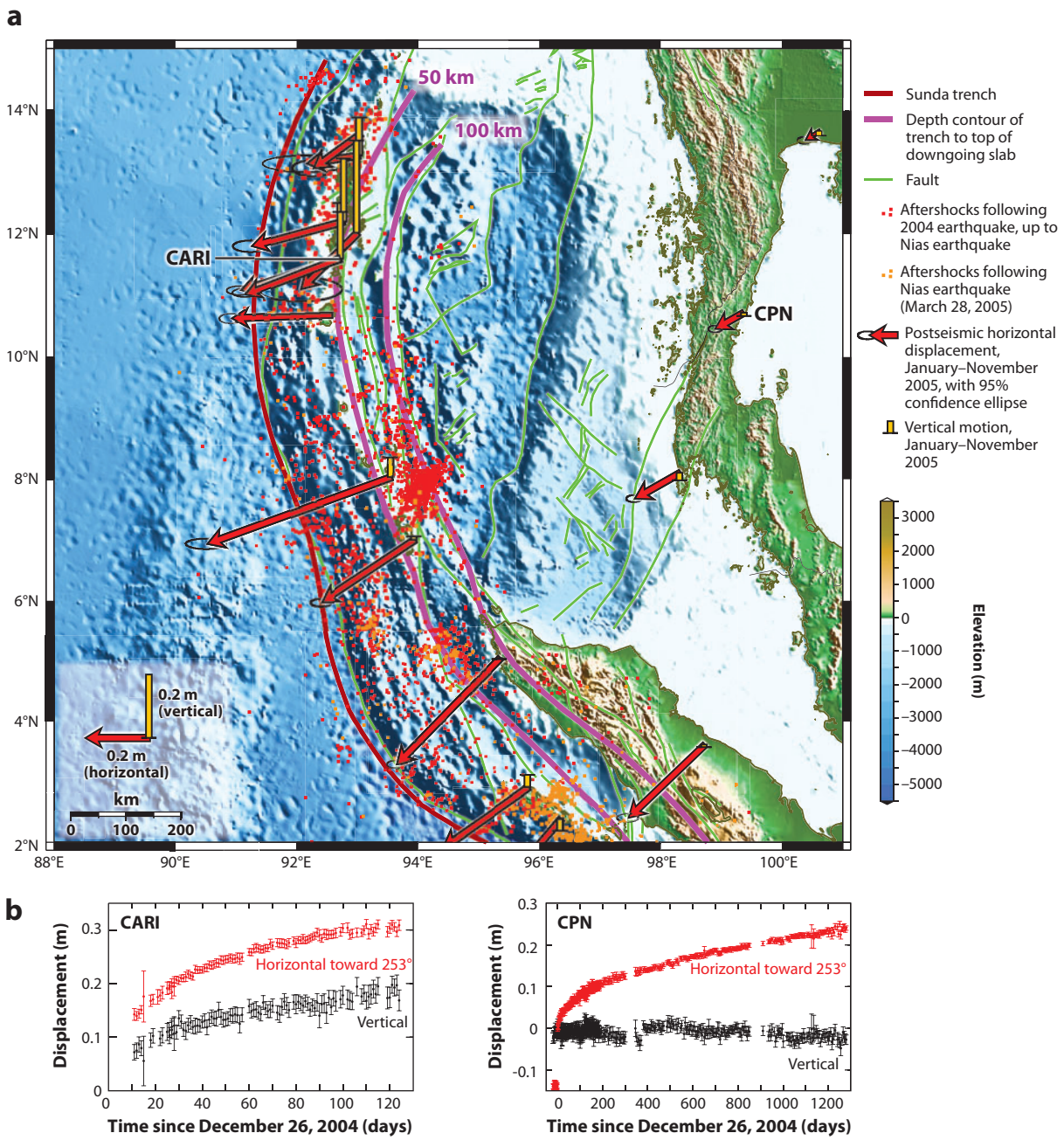

Figure 8

(*a*) Map of GPS-measured postseismic displacements from January to November of 2005. Contributions from interseismic deformation and coseismic offsets from the 2005 Nias earthquake have been removed. Depth contours are from Gudmundsson & Sambridge 1998. Faults are after Curray 2005. Arrows show the GPS-measured horizontal postseismic displacements from January to November of 2005. Vertical bars represent the vertical motions during the same time. (*b*) Time series (*graphs*) show postseismic motions of station CPN in Chumpon, Thailand (data courtesy of NICT and M. Hashimoto) and CARI at Port Blair on south Andaman Island (data courtesy J. Paul, CERI) with interseismic trends removed from horizontal components.

west as in the earthquake, but partially reversed their coseismic subsidence (Banerjee et al. 2007, Gahalaut et al. 2008a, Paul et al. 2007). Continuous and survey-mode GPS data from the islands support the view that postseismic deformation in the first months following the earthquake included a contribution from rapid afterslip downdip of the coseismic rupture (Banerjee et al. 2007, Paul et al. 2007). A much more optimally distributed GPS network spanning the subsequent rupture of the 2005 Nias earthquake also documents rapid deformation transients that are well explained by postseismic afterslip both up- and downdip of the coseismic rupture (Hsu et al. 2006).

Continuous GPS sites at greater distances in eastern Sumatra and Thailand also show a pronounced acceleration of motion toward the southwest following the 2004 earthquake, with rates of up to ~500 mm year^{-1} during the first three months (Hashimoto et al. 2006, Pollitz et al. 2006a). Postseismic displacements at sites in western Thailand already exceed their coseismic offsets. For example, station CPN in Chumpon, Thailand, displaced horizontally by 0.14 m during the earthquake and continued at a rapid pace for 0.24 m above and beyond expected interseismic motions to the southwest by July 2009 (see **Figure 8**). The magnitude and direction of accelerated motion agree with the predictions of viscoelastic relaxation models (Pollitz et al. 2006a, 2008) but can also be reproduced by kinematic models of substantial afterslip (Hashimoto et al. 2006).

In addition to other participating relaxation processes (afterslip and poroelastic rebound), events of this magnitude are followed by viscous relaxation of coseismic stress changes involving the crystal plastic deformation of rocks (Bürgmann & Dresen 2008). Models of upper mantle relaxation in a spherical, stratified Earth predict substantial postseismic effects over a wide region surrounding the eastern Indian Ocean (Pollitz et al. 2006a, 2008). **Figure 9** shows the predicted displacements for a 60-year period following the 2004 Sumatra earthquake from viscoelastic relaxation in the mantle using a model with a viscosity structure deduced from the observed GPS time series during the first year of postseismic motion (Pollitz et al. 2006a). Whereas details of the ultimate postseismic displacements in the region will depend on the nature and distribution of rheological properties of both the plate interface and the underlying mantle, the eventual magnitude of transient motions at far-field distances will be of the order shown in **Figure 9**. Owing to the depth extent of this relaxation, postseismic surface displacements in the far field will greatly exceed static coseismic displacements (compare **Figures 3** and **9**). Consideration of near- and far-field GPS data, horizontal and vertical transient motions, and of the postseismic gravity changes discussed below promises to resolve the contributions from the different postseismic relaxation processes to the observed deformation transients.

The relaxation processes following the Sumatra earthquake also produced a notable time-varying gravity field that was captured by the GRACE satellite mission. Whereas the coarse spatial resolution and overlapping contributions from hydrological changes complicate the analysis, the spatial and temporal patterns captured by the gravity measurements may lend additional diagnostic power to efforts focused on separating contributions from afterslip, poroelastic rebound, and viscoelastic relaxation. The lateral extent of the postseismic signal is consistent with deformation processes acting quite deep in Earth. Ogawa & Heki (2007) suggested that poroelastic rebound associated with fluid flow in the upper mantle can produce the postseismic gravity changes. They argued that sufficient amounts of water exist in the mantle and that permeabilities may be high enough to produce the observed signal. Panet et al. (2007) and Han et al. (2008) suggested that the broad postseismic gravity increase is consistent with rapid viscous relaxation such as that produced by a biviscous Burgers body with a rapidly decaying low-viscosity element (~10^{17} Pa s) and a higher (~10^{19} Pa s) longer-term viscosity consistent with that found by Pollitz et al. (2006a).

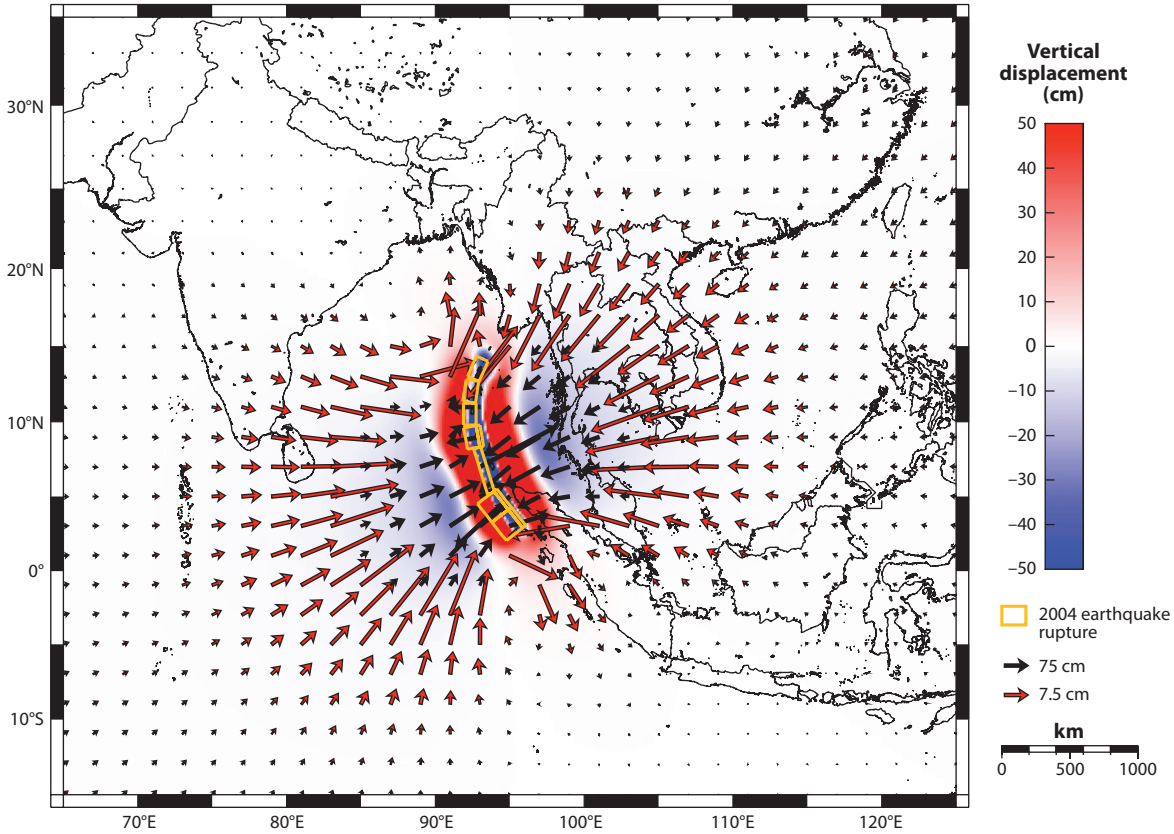

Figure 9

Predicted horizontal and vertical motions from mantle relaxation following the 2004 earthquake. Cumulative transient motions 60 years after the earthquakes will ultimately amount to more than 50 cm, up to distances of approximately 1000 km from the rupture in the southwest and northeast directions. This prediction is based on an optimal biviscous mantle rheology model derived from early postseismic GPS data (Pollitz et al. 2006a).

The extensive and far-reaching deformation transients from the 2004/2005 Sumatra-Andaman ruptures will impact the loading and earthquake occurrence on many other faults, even at very large distances. Depending on the rheology of the asthenosphere, measurable deformation pulses from megathrust earthquakes may travel thousands of kilometers and impact seismicity at great distances and for many decades (Pollitz et al. 1998). The occurrence of the March 28, 2005, M_W 8.7 Nias earthquake likely was hastened by a combination of coseismic and postseismic stress transients from the December 26, 2004, event (Nalbant et al. 2005, Pollitz et al. 2006b), and stress changes from the 2004/2005 events may have significantly increased seismic activity along the Sumatra-Andaman-Sagaing fault system (Cattin et al. 2009). Given that deformation landward of the 1960 Chile and 1964 Alaska earthquake is still dominated by postseismic transient motions nearly 50 years after these megathrust events (Khazaradze et al. 2002, Zweck et al. 2002), the Sumatra-Andaman earthquake is likely to have modified crustal deformation patterns in the region for decades to come. Space geodesy and advanced models of relevant deformation processes provide a unique opportunity to monitor the perturbations to the regional strain field following

the Sumatra-Andaman earthquake and to quantitatively gauge stress changes on the adjacent segments of the Sunda subduction system, the Sumatra-Andaman-Sagaing fault system, along the Himalaya, and in the western Pacific subduction zones.

Past Megathrust Events on the Sunda-Andaman Subduction Zone

The Indian Ocean tsunami of December 26, 2004, reached maximum wave heights of 30 to 50 m in Aceh, and there are no historic records of similarly large tsunamis or earthquakes in the eastern Indian Ocean. However, recent excavations of coastal deposits in Aceh province of northern Sumatra reveal extensive sand sheets with similar sediment characteristics to those laid down in 2004, deposited soon after AD 1290–1400 and AD 780–990, that likely resulted from earlier tsunamis (Monecke et al. 2008). Near Phuket, Thailand, Jankaew et al. (2008) also examined sedimentary evidence for tsunamis and identified two probable precedents for the 2004 tsunami at a grassy beach-ridge plain 125 km north of Phuket, less than 2800 years old. The most recent full-size predecessor at this site to the 2004 tsunami occurred at approximately AD 1300–1450. Thus, it does appear that prior occurrences of 2004-sized events did occur, but these occurred too long ago to have been noted in historic records.

M_W 7.7 to 7.9 earthquakes occurred within the 2004 rupture zone in 1881 and 1941 (see **Figure 1**), which generated small tsunamis (Bilham 2005). Further south along the Sunda arc, a number of large earthquakes are known from historical accounts, including an $M_W \sim 9$ event in 1833. Studies of sea-level changes recorded in corals can extend the record back much further and suggest that sequences of great earthquakes have occurred south of Aceh approximately every two centuries for at least the past 700 years (Sieh et al. 2008). The occurrence of the 2007 M_W 7.9 and 8.4 earthquakes in the Mentawai patch, together with the 2005 M_W 8.6 Nias earthquake to the north, raises obvious concern that a larger earthquake on the Mentawai region may strike within the next few decades (Sieh et al. 2008). A tsunami from such an event could prove even more deadly than the 2004 tsunami, given the large population of Padang and other cities along the western coast of Sumatra.

Despite a prescient warning by Cummins (2004) about the tsunami hazard of the Sunda subduction zone, the occurrence of the 2004 Sumatra-Andaman earthquake came as a surprise to many geophysicists because only $M_W < 8$ earthquakes had been recorded in the region, and catalogued $M_W > 9$ earthquakes had occurred in areas with young oceanic crust subducting at high rates (Ruff & Kanamori 1980). It appears that we simply have too few examples of great megathrust earthquakes, particularly from regions with long repeat times, to make reliable generalizations about maximum expected earthquake size. In this respect, it is sobering that further southeast from Sumatra along the Sunda arc is the heavily populated island of Java. Like the Andaman section, the subduction rate here is slow, and it was not thought that the region was at large risk for a great earthquake. Following the 2004 Sumatra-Andaman earthquake, however, it can now be argued that this section of the subduction zone is one of the world's most hazardous, given the size of its population exposure (McCaffrey 2008). Conversely, GPS-measured interseismic velocities of three sites in Java show little arc-normal motion (Socquet et al. 2006) and suggest a rather narrow locked zone along this section of the megathrust. Another region with unknown but potentially large risk is north of the Andaman Islands, along the Burma coast, where historical and geodetic evidence suggests megathrust earthquakes and tsunamis are possible (Cummins 2007). Understanding the earthquake potential along the whole megathrust is important, which will require both improved characterization of the active elastic strain field and a more complete examination of past earthquake behavior.

SUMMARY POINTS

1. The 2004 Sumatra-Andaman earthquake produced huge geophysical signals with worldwide impact, including seismic and tsunami waves, static displacements, and gravity changes. These have triggered and will continue to trigger seismic and volcanic activity, as stress and geodetic changes will persist for many years from postseismic relaxation processes.
2. The earthquake rupture was complex in its details, and different studies have not reached full agreement regarding its total moment, rupture velocity, fault geometry, and slip distribution. However, there is no convincing evidence that the event involved any exotic phenomena, such as slow slip, that are not commonly observed for other large earthquakes.
3. The variability of slip in the event may reflect changes in convergence rate, the degree of seismic coupling, and/or the slip history in previous events.
4. Simple relations between rate, slab age, or structure of a subduction zone and the maximum size of events can be misleading. Only in hindsight have we found geologic and geophysical evidence that shows that the Sumatra-Andaman subduction thrust is capable of generating $M > 9$ megathrust events. Thus all areas of active subduction should be considered at risk of great earthquakes.

FUTURE ISSUES

1. Coseismic slip may have occurred in part on secondary faults within the accretionary wedge, but it is difficult to resolve this from the available seismic and geodetic data.
2. Far-reaching postseismic deformation transients likely include contributions from both afterslip and viscous relaxation. These transients will impact deformation and stress rates and thus seismic hazard in the region for decades to come.
3. Improved methods to quickly estimate earthquake size and tsunami potential worldwide are needed to help provide better advance warning of the hazard from future megathrust earthquakes.

DISCLOSURE STATEMENT

The authors are not aware of any affiliations, memberships, funding, or financial holdings that might be perceived as affecting the objectivity of this review.

ACKNOWLEDGMENTS

We are very grateful to contributions from Martin Mai, who compiled and plotted the different models shown in **Figure 6**. Kelly Grijalva created **Figure 5**, and the gravity data shown in **Figure 3** are courtesy of John Wahr and Sean Swenson. The Alexander von Humboldt Stiftung supported a visit by R.B. at the University of München during which the article was written.

LITERATURE CITED

Abe K. 1979. Size of great earthquakes of 1837–1974 inferred from tsunami data. *J. Geophys. Res.* 84:1561–68

Ammon CJ, Ji C, Thio HK, Robinson D, Ni SD, et al. 2005. Rupture process of the 2004 Sumatra-Andaman earthquake. *Science* 308:1133–39

Araki E, Shinohara M, Obana K, Yamada T, Kaneda Y, et al. 2006. Aftershock distribution of the 26 December 2004 Sumatra-Andaman earthquake from ocean bottom seismographic observation. *Earth Planet. Space* 58:113–19

Banerjee P. 2005. Interseismic geodetic motion and far-field coseismic surface displacements caused by the 26 December 2004 Sumatra earthquake observed from GPS data. *Curr. Sci.* 88:1491–96

Banerjee P, Pollitz F, Bürgmann R. 2005. The size and duration of the Sumatra-Andaman earthquake from far-field static offsets. *Science* 308:1769–72

Banerjee P, Pollitz FF, Nagarajan B, Bürgmann R. 2007. Coseismic slip distributions of the 26 December 2004 Sumatra-Andaman and 28 March 2005 Nias earthquakes from GPS static offsets. *Bull. Seismol. Soc. Am.* 97:S86–102

Bilek SL. 2007. Using earthquake source durations along the Sumatra-Andaman subduction system to examine fault-zone variations. *Bull. Seismol. Soc. Am.* 97:S62–70

Bilham R. 2005. A flying start, then a slow slip. *Science* 308:1126–27

Bilham RG, Engdahl ER, Feldl N, Satyabala SP. 2005. Partial and complete rupture of the Indo-Andaman plate boundary 1847–2004. *Seismol. Res. Lett.* 76:299–311

Blewitt G, Kreemer C, Hammond WC, Plag HP, Stein S, Okal E. 2006. Rapid determination of earthquake magnitude using GPS for tsunami warning systems. *Geophys. Res. Lett.* 33:L11309

Braitenberg C, Zadro M. 2007. Comparative analysis of the free oscillations generated by the Sumatra-Andaman Islands 2004 and the Chile 1960 earthquakes. *Bull. Seismol. Soc. Am.* 97:S6–17

Briggs RW, Sieh K, Meltzner AJ, Natawidjaja D, Galetzka J, et al. 2006. Deformation and slip along the Sunda Megathrust in the great 2005 Nias-Simeulue earthquake. *Science* 311:1897–901

Bürgmann R, Dresen G. 2008. Rheology of the lower crust and upper mantle: evidence from rock mechanics, geodesy and field observations. *Annu. Rev. Earth Planet. Sci.* 36:531–67

Cattin R, Chamot-Rooke N, Pubellier M, Rabaute A, Delescluse M, et al. 2009. Stress change and effective friction coefficient along the Sumatra-Andaman-Sagaing fault system after the 26 December 2004 ($M_w = 9.2$) and the 28 March 2005 ($M_w = 8.7$) earthquakes. *Geochem. Geophys. Geosyst.* 10:Q03011

Chen JL, Wilson CR, Tapley BD, Grand S. 2007. GRACE detects coseismic and postseismic deformation from the Sumatra-Andaman earthquake. *Geophys. Res. Lett.* 34:L13302

Chlieh M, Avouac J-P, Hjorleifsdottir V, Song T-R, Ji C, et al. 2007. Coseismic slip and afterslip of the great (M_w 9.15) Sumatra-Andaman earthquake of 2004. *Bull. Seismol. Soc. Am.* 97:S152–73

Choy GL, Boatwright J. 2007. The energy radiated by the 26 December 2004 Sumatra-Andaman earthquake estimated from 10-minute P-wave windows. *Bull. Seismol. Soc. Am.* 97:S18–24

Cifuentes IL, Silver PG. 1989. Low-frequency source characteristics of the great 1960 Chilean earthquake. *J. Geophys. Res.* 94(B1):643–63

Cummins P. 2004. Small threat, but warning sounded for tsunami research. *Aus. Geo. News* 75:4–7

Cummins PR. 2007. The potential for giant tsunamigenic earthquakes in the northern Bay of Bengal. *Nature* 449:75–78

Curray JR. 2005. Tectonics and history of the Andaman Sea region. *J. Asian Earth Sci.* 25:187–232

de Groot-Hedlin CD. 2005. Estimation of the rupture length and velocity of the Great Sumatra earthquake of Dec 26, 2004 using hydroacoustic signals. *Geophys. Res. Lett.* 32:L11303

de Linage C, Rivera L, Hinderer J, Boy JP, Rogister Y, et al. 2009. Separation of coseismic and postseismic gravity changes for the 2004 Sumatra-Andaman earthquake from 4.6 yr of GRACE observations and modelling of the coseismic change by normal-modes summation. *Geophys. J. Int.* 176:695–714

Delescluse M, Chamot-Rooke N. 2006. Instantaneous deformation and kinematics of the India-Australia plate. *Geophys. J. Int.* 168:818–42

Dewey JW, Choy G, Presgrave B, Sipkin S, Tarr AC, et al. 2007. Seismicity associated with the Sumatra-Andaman Islands earthquake of 26 December 2004. *Bull. Seismol. Soc. Am.* 97:S25–42

Engdahl ER, Villasenor A, DeShon HR, Thurber CH. 2007. Teleseismic relocation and assessment of seismicity (1918–2005) in the region of the 2004 M_w 9.0 Sumatra-Andaman and 2005 M_w 8.6 Nias Island great earthquakes. *Bull. Seismol. Soc. Am.* 97:S43–61

Fujii Y, Satake K. 2007. Tsunami source of the 2004 Sumatra-Andaman earthquake inferred from tide gauge and satellite data. *Bull. Seismol. Soc. Am.* 97:S192–207

Gahalaut VK, Catherine JK, Jade S, Gireesh R, Gupta DC, et al. 2008a. No evidence of unusually large postseismic deformation in Andaman region immediately after 2004 Sumatra-Andaman earthquake. *Geophys. Res. Lett.* 35:L10307

Gahalaut VK, Jade S, Catherine JK, Gireesh R, Ananda MB, et al. 2008b. GPS measurements of postseismic deformation in the Andaman-Nicobar region following the giant 2004 Sumatra-Andaman earthquake. *J. Geophys. Res.* 113:B08401

Gahalaut VK, Nagarajan B, Catherine JK, Kumar S. 2006. Constraints on 2004 Sumatra-Andaman earthquake rupture from GPS measurements in Andaman-Nicobar islands. *Earth Planet. Sci. Lett.* 242:365–74

Geist EL, Titov VV, Arcas D, Pollitz FF, Bilek SL. 2007. Implications of the 26 December 2004 Sumatra-Andaman earthquake on tsunami forecast and assessment models for great subduction-zone earthquakes. *Bull. Seismol. Soc. Am.* 97:S249–70

Gudmundsson O, Sambridge M. 1998. A regionalized upper mantle (RUM) model. *J. Geophys. Res.* 103:7121–36

Guilbert J, Vergoz J, Schissele E, Roueff A, Cansi Y. 2005. Use of hydroacoustic and seismic arrays to observe rupture propagation and source extent of the $M_w = 9.0$ Sumatra earthquake. *Geophys. Res. Lett.* 32:L15310

Gusev AA, Guseva EM, Panza GF. 2007. Size and duration of the high-frequency radiator in the source of the 2004 December 26 Sumatra earthquake. *Geophys. J. Int.* 170:1119–28

Han SC, Sauber J, Luthcke SB, Ji C, Pollitz FF. 2008. Implications of postseismic gravity change following the great 2004 Sumatra-Andaman earthquake from the regional harmonic analysis of GRACE intersatellite tracking data. *J. Geophys. Res.* 113:B11413

Han SC, Shum CK, Bevis M, Ji C, Kuo CY. 2006. Crustal dilatation observed by GRACE after the 2004 Sumatra-Andaman earthquake. *Science* 313:658–62

Hashimoto M, Choosakul N, Hashizume M, Takemoto S, Takigucki H, et al. 2006. Crustal deformations associated with the great Sumatra-Andaman earthquake deduced from continuous GPS observation. *Earth Planet. Space* 58:127–39

Hayes GP, Wald DJ. 2009. Developing framework to constrain the geometry of the seismic rupture plane on subduction interfaces a priori: a probabilistic approach. *Geophys. J. Int.* 176:951–64

Houston H, Kanamori H. 1986. Source spectra of great earthquakes: teleseismic constraints on rupture process and strong motion. *Bull. Seismol. Soc. Am.* 76:19–42

Hsu YJ, Simons M, Avouac JP, Galetzka J, Sieh K, et al. 2006. Frictional afterslip following the 2005 Nias-Simeulue earthquake, Sumatra. *Science* 312:1921–26

Ishii M, Shearer PM, Houston H, Vidale JE. 2005. Extent, duration and speed of the 2004 Sumatra-Andaman earthquake imaged by the Hi-Net array. *Nature* 435:933–36

Ito Y, Obara K, Shiomi K, Sekine S, Hirose H. 2007. Slow earthquakes coincident with episodic tremors and slow slip events. *Science* 315:503–6

Jade S, Ananda M, Kumar P, Banerjee S. 2005. Co-seismic and post-seismic displacements in Andaman and Nicobar islands from GPS measurements. *Curr. Sci.* 88:1980–84

Jankaew K, Atwater BF, Sawai Y, Choowong M, Charoentitirat T, et al. 2008. Medieval forewarning of the 2004 Indian Ocean tsunami in Thailand. *Nature* 455:1228–31

Kanamori H. 2006a. Lessons from the 2004 Sumatra-Andaman earthquake. *Philos. Trans. R. Soc. A* 364:1927–45

Kanamori H. 2006b. Seismological aspects of the December 2004 great Sumatra-Andaman earthquake. *Earthq. Spectra* 22:S1–12

Kanamori H. 2006c. The radiated energy of the 2004 Sumatra-Andaman earthquake. In *Earthquakes: Radiated Energy and the Physics of Faulting*, ed. R Abercrombie, A McGarr, H Kanamori, G Di Toro, pp. 59–68. AGU Geophys. Monogr. Ser. 170. Washington, DC: AGU

Kayanne H, Ikeda Y, Echigo T, Shishikura M, Kamataki T, et al. 2007. Coseismic and postseismic creep in the Andaman Islands associated with the 2004 Sumatra-Andaman earthquake. *Geophys. Res. Lett.* 34:L01310

Khazaradze G, Wang K, Klotz J, Hu Y, He J. 2002. Prolonged post-seismic deformation of the 1960 great Chile earthquake and implications for mantle rheology. *Geophys. Res. Lett.* 29:2050

Konca AO, Avouac J-P, Sladen A, Meltzner AJ, Sieh K, et al. 2008. Partial rupture of a locked patch of the Sumatra megathrust during the 2007 earthquake sequence. *Nature* 456:631–35

Kreemer C, Blewitt G, Hammond WC, Plag HP. 2006. Global deformation from the great 2004 Sumatra-Andaman Earthquake observed by GPS: implications for rupture process and global reference frame. *Earth Planet. Space* 58:141–48

Kruger F, Ohrnberger M. 2005a. Spatio-temporal source characteristics of the 26 December 2004 Sumatra earthquake as imaged by teleseismic broadband arrays. *Geophys. Res. Lett.* 32:L24312

Kruger F, Ohrnberger M. 2005b. Tracking the rupture of the $M_w = 9.3$ Sumatra earthquake over 1150 km at teleseismic distance. *Nature* 435:937–39

Lambotte S, Rivera L, Hinderer J. 2006. Rupture length and duration of the 2004 Aceh-Sumatra earthquake from the phases of the Earth's gravest free oscillations. *Geophys. Res. Lett.* 33:L03307

Lambotte S, Rivera L, Hinderer J. 2007. Constraining the overall kinematics of the 2004 Sumatra and the 2005 Nias earthquakes using the earth's gravest free oscillations. *Bull. Seismol. Soc. Am.* 97:S128–38

Langbein J, Murray JR, Snyder HA. 2006. Coseismic and initial postseismic deformation from the 2004 Parkfield, California, earthquake, observed by global positioning system, electronic distance meter, creepmeters, and borehole strainmeters. *Bull. Seismol. Soc. Am.* 96:S304–20

Lay T, Kanamori H, Ammon CJ, Nettles M, Ward SN, et al. 2005. The great Sumatra-Andaman earthquake of December 26, 2004. *Science* 308:1127–33

Lomax A. 2005. Rapid estimation of rupture extent for large earthquakes: application to the 2004, M9 Sumatra-Andaman mega-thrust. *Geophys. Res. Lett.* 32:L10314

Masterlark T, Hughes KLH. 2008. Next generation of deformation models for the 2004 M9 Sumatra-Andaman earthquake. *Geophys. Res. Lett.* 35:L19310

McCaffrey R. 2008. Global frequency of magnitude 9 earthquakes. *Geology* 36:263–66

McCaffrey R. 2009. The tectonic framework of the Sumatran subduction zone. *Annu. Rev. Earth Planet. Sci.* 37:345–66

Meltzner A, Sieh K, Abrams M, Agnew DC, Hudnut KW, et al. 2006. Uplift and subsidence associated with the great Aceh-Andaman earthquake of 2004. *J. Geophys. Res.* 111:B02407

Monecke K, Finger W, Klarer D, Kongko W, McAdoo BG, et al. 2008. A 1000-year sediment record of tsunami recurrence in northern Sumatra. *Nature* 455:1232–34

Nalbant SS, Steacy S, Sieh K, Natawidjaja D, McCloskey J. 2005. Earthquake risk on the Sunda trench. *Nature* 435:756–57

Natawidjaja DH, Sieh K, Chlieh M, Galetzka J, Suwargadi BW, et al. 2006. Source parameters of the great Sumatran megathrust earthquakes of 1797 and 1833 inferred from coral microatolls. *J. Geophys. Res.* 111:B06403

Neetu S, Suresh I, Shankar R, Shankar D, Shenoi SSC, et al. 2005. Comment on "The great Sumatra-Andaman earthquake of 26 December 2004." *Science* 310:1431

Ni S, Kanamori H, Helmberger D. 2005. Seismology: energy radiation from the Sumatra earthquake. *Nature* 434:582

Ogawa R, Heki K. 2007. Slow postseismic recovery of geoid depression formed by the 2004 Sumatra-Andaman earthquake by mantle water diffusion. *Geophys. Res. Lett.* 34:L06313

Panet I, Mikhailov V, Diament M, Pollitz F, King G, et al. 2007. Coseismic and post-seismic signatures of the Sumatra 2004 December and 2005 March earthquakes in GRACE satellite gravity. *Geophys. J. Int.* 171:177–90

Paul J, Lowry AR, Bilham R, Sen S, Smalley R. 2007. Postseismic deformation of the Andaman Islands following the 26 December, 2004 Great Sumatra-Andaman earthquake. *Geophys. Res. Lett.* 34:L19309

Piatanesi A, Lorito S. 2007. Rupture process of the 2004 Sumatra-Andaman earthquake from tsunami waveform inversion. *Bull. Seismol. Soc. Am.* 97:S223–31

Pietrzak J, Socquet A, Ham D, Simons W, Vigny C, et al. 2007. Defining the source region of the Indian Ocean Tsunami from GPS, altimeters, tide gauges and tsunami models. *Earth Planet. Sci. Lett.* 261:49–64

Plafker G, Nishenko S, Cluff L, Syahrial M. 2006. The cataclysmic 2004 tsunami on NW Sumatra: preliminary evidence for a near-field secondary source along the western Aceh basin. *Seismol. Res. Lett.* 77:231 (Abstr.)

Pollitz F, Banerjee P, Grijalva K, Nagarajan B, Burgmann R. 2008. Effect of 3-D viscoelastic structure on post-seismic relaxation from the 2004 M = 9.2 Sumatra earthquake. *Geophys. J. Int.* 173:189–204

Pollitz F, Bürgmann R, Banerjee P. 2006a. Postseismic relaxation following the great 2004 Sumatra-Andaman earthquake on a compressible self-gravitating Earth. *Geophys. J. Int.* 167:397–420

Pollitz F, Bürgmann R, Romanowicz B. 1998. Viscosity of oceanic asthenosphere inferred from remote triggering of earthquakes. *Science* 280:1245–49

Pollitz FF, Banerjee P, Bürgmann R, Hashimoto M, Chhoosakul N. 2006b. Stress changes along the Sunda trench following the 26 December 2004 Sumatra-Andaman and 28 March 2005 Nias earthquakes. *Geophys. Res. Lett.* 33:L06309

Rhie J, Dreger DS, Bürgmann R, Romanowicz B. 2007. Slip of the 2004 Sumatra-Andaman earthquake from joint inversion of long period global seismic waveforms and GPS static offsets. *Bull. Seismol. Soc. Am.* 97:S115–27

Rogers G, Dragert H. 2003. Episodic tremor and slip on the Cascadia subduction zone: the chatter of silent slip. *Science* 300:1942–43

Ruff L, Kanamori H. 1980. Seismicity and the subduction process. *Phys. Earth Planet. Int.* 23:240–52

Satake K, Atwater BF. 2007. Long-term perspectives on giant earthquakes and tsunamis at subduction zones. *Annu. Rev. Earth Planet. Sci.* 35:349–74

Segall P, Davis JL. 1997. GPS applications for geodynamics and earthquake studies. *Annu. Rev. Earth Planet. Sci.* 25:301–36

Sibuet JC, Rangin C, Le Pichon X, Singh S, Cattaneo A, et al. 2007. 26th December 2004 great Sumatra-Andaman earthquake: co-seismic and post-seismic motions in northern Sumatra. *Earth Planet. Sci. Lett.* 263:88–103

Sieh K, Natawidjaja DH, Meltzner AJ, Shen C-C, Cheng H, et al. 2008. Earthquake supercycles inferred from sea-level changes recorded in the corals of West Sumatra. *Science* 322:1674–78

Singh SC, Carton H, Tapponnier P, Hananto ND, Chauhan APS, et al. 2008. Seismic evidence for broken oceanic crust in the 2004 Sumatra earthquake epicentral region. *Nat. Geosci.* 1:777–81

Socquet A, Vigny C, Chamot-Rooke N, Simons W, Rangin C, Ambrosius B. 2006. India and Sunda plates motion and deformation along their boundary in Myanmar determined by GPS. *J. Geophys. Res.* 111:B05406

Song YT, Ji C, Fu L-L, Zlotnicki V, Shum CK, et al. 2005. The 26 December 2004 tsunami source estimated from satellite radar altimetry and seismic waves. *Geophys. Res. Lett.* 32:L20601

Stein S, Okal EA. 2005. Speed and size of the Sumatra earthquake. *Nature* 434:581–82

Stein S, Okal EA. 2007. Ultralong period seismic study of the December 2004 Indian Ocean earthquake and implications for regional tectonics and the subduction process. *Bull. Seismol. Soc. Am.* 97:S279–95

Subarya C, Chlieh M, Prawirodirdjo L, Avouac JP, Bock Y, et al. 2006. Plate-boundary deformation associated with the great Sumatra-Andaman earthquake. *Nature* 440:46–51

Titov V, Rabinovich AB, Mofjeld HO, Thomson RE, Gonzalez FI. 2005. The global reach of the 26 December 2004 Sumatra tsunami. *Science* 309:2045–48

Tolstoy M, Bohnenstiehl DR. 2005. Hydroacoustic constraints on the rupture duration, length, and speed of the great Sumatra-Andaman earthquake. *Seismol. Res. Lett.* 76:419–25

Tolstoy M, Bohnenstiehl DR. 2006. Hydroacoustic contributions to understanding the December 26th 2004 great Sumatra-Andaman Earthquake. *Surv. Geophys.* 27:633–46

Tsai VC, Nettles M, Ekstrom G, Dziewonski AM. 2005. Multiple CMT source analysis of the 2004 Sumatra earthquake. *Geophys. Res. Lett.* 32:L17304

Vallee M. 2007. Rupture properties of the giant Sumatra earthquake imaged by empirical Green's function analysis. *Bull. Seismol. Soc. Am.* 97:S103–14

Vigny C, Simons WJF, Abu S, Bamphenyu R, Satirapod C, et al. 2005. Insight into the 2004 Sumatra-Andaman earthquake from GPS measurements in southeast Asia. *Nature* 436:201–6

Zweck C, Freymueller JT, Cohen SC. 2002. The 1964 great Alaska earthquake: present day and cumulative postseismic deformation in the western Kenai Peninsula. *Phys. Earth Planet. Int.* 132:5–20